Katholieke *Universiteit* Nijmegen

Dynamics of HF and HCl dimers

Hoofdvak verslag Informatische Chemie

G.W.M. Vissers

November 25, 1999

Institute of Theoretical Chemistry
Toernooiveld 1
Nijmegen

Katholieke *Universiteit* Nijmegen

Dynamics of HF and HCl dimers

Hoofdvak verslag Informatische Chemie

G.W.M. Vissers

November 25, 1999

Institute of Theoretical Chemistry
Toernooiveld 1
Nijmegen

Samenvatting

Dit verslag behandelt de theorie en resultaten van quantummechanische berekeningen aan HX ($X = \mathrm{Cl}, \mathrm{F}$) dimeren. Het werk is gedaan in het kader van een hoofdvakstage Informatische Chemie op de afdeling Theoretische Chemie aan de Katholieke Universiteit Nijmegen.

De behandelde HX dimeren bestaan uit twee HX moleculen die bij elkaar gehouden worden door een waterstofbinding. Het probleem dat is aangepakt is het berekenen van de energieniveaus en golffuncties van het dimeer in de grondtoestand, en in de toestand waarin één van de monomeren vibrationeel aangeslagen is. Dit is gedaan door diagonalisatie van de Hamiltoniaan in een basis voor alle zes interne coördinaten. Deze coördinaten zijn de twee intramoleculaire afstanden, de afstand tussen de twee moleculen en drie interne hoeken. De gebruikte basis is aangepast aan de symmetrie in het dimeer.

Voor het potentiële energie gedeelte in de Hamiltoniaan zijn verschillende potentiaaloppervlakken bestudeerd. Voor één van deze oppervlakken, het $SO{-}3$ opervlak voor het HF dimeer, zijn er nog geen resultaten gepubliceerd. Verder zijn er voor de grondtoestandsberekeningen in de monomeer vibratie basis twee soorten functies gebruikt, namelijk basisfuncties die afgeleid zijn van het vrije monomeer en basisfuncties die aangepast zijn aan het dimeer.

De resultaten voor de berekeningen aan de vibrationele grondtoestand komen tamelijk goed overeen met waarden uit de literatuur. De meeste afwijkingen zijn te verklaren uit het gebruik van een grotere monomeer vibratie basis in de berekeningen uit dit verslag. Voor $(\mathrm{HCl})_2$ blijkt het aanpassen van de monomeer vibratie functies aan het dimeer nauwelijks effect te hebben op de energieniveaus. Voor $(\mathrm{HF})_2$ is er wel een effect merkbaar bij gebruik van het $SQSBDE$ potentiaaloppervlak, maar geen bij SO–3 opervlak. Tenslotte blijkt dat de SO–3 potentiaal de dissociatie energie en de splisingen tussen de energieniveaus in vergelijking met experimentele resultaten beter reproduceert dan het $SQSBDE$ oppervlak.

Bij het berekenen van de aangeslagen toestand kon geen gebruik meer worden gemaakt van het iteratieve algoritme dat in de grondtoestandsberekeningen werd gebruikt. Een oplossing is gevonden in prediagonalisatie van de blokken van de Hamiltoniaan die diagonaal zijn in de monomeer vibratie functies, en het gebruik van een deel van de resulterende eigenfuncties voor een nieuwe, gereduceerde basis. Bij het selecteren van de functies voor deze basis is echter alleen gekeken naar het effect dat deze functies hebben op de vibrationeel aangeslagen toestanden, zonder rekening te houden met de hooggelegen vibrationele grondtoestanden. Daardoor zijn (onder andere) de energieniveaus van de grondtoestandsfuncties die in de buurt liggen van de excitatie energie verschoven ten opzichte van de waarde die zij bij gebruik van een ongereduceerde basis zouden hebben. Voor $(\mathrm{HCl})_2$ heeft dit geen erg grote gevolgen; de aangslagen toestanden zijn tamelijk goed

geconvergeerd. De berekende splitsingen komen dan ook erg goed overeen met de literauur. Voor $(HF)_2$ heeft de verschuiving echter een groter effect, doordat sommige hooggelegen grondtoestandsniveaus erg dicht in de buurt komen van bepaalde aangeslagen toestanden. Hierdoor mengen de betreffende vibrationele grondtoestand en aangeslagen toestand sterk, wat een verstoring van beide niveaus ten gevolge heeft. Door dit effect is de onzekerheid in de berekende aangeslagen HF dimeer energieën erg groot. Desondanks komen de splitsingen redelijk goed overeen met de literatuurwaarden. Ook voor de aangeslagen toestand blijkt dat de SO–3 potentiaal de splitsingen beter reproduceert dan de $SQSBDE$ potentiaal.

Voor de aangeslagen toestanden moeten nieuwe berekeningen gedaan worden, waarbij het effect van de reductie van de basis op de grondtoestandsniveaus in de buurt van de aangeslagen energieën geminimaliseerd wordt. Alle berekeningen in dit verslag zijn gedaan voor een totaal hoekmoment $J = 0$. Toekomstige berekeningen zouden ook voor hogere J uitgevoerd kunnen worden, waarbij misschien het effect van Coriolis koppeling moet worden meegenomen.

Dankwoord

Op deze plaats zou ik graag iedereen van de afdeling willen bedanken voor alle steun die ik tijdens mijn stage heb mogen ontvangen. Ad van der Avoird en Gerrit Groenenboom wil ik bedanken voor hun begeleiding. Paul Wormer wil ik bedanken voor het kritisch doorlezen van, en het commentaar leveren op, dit verslag. Ook Ine Meijer wil ik hartelijk bedanken voor het oplossen van nagenoeg alle problemen die niet met de theorie te maken hebben.

Verdere dank gaat uit naar Michel Geleijns, Mirjam van Vroonhoven en Wilfried Zeimen, die elk in meer of mindere mate een bijdrage hebben geleverd in het wegwijs maken op de afdeling en het voeren van (soms) nuttige discussies.

Tenslotte wil ik mijn familie en mijn vriendin bedanken voor alles wat zij gedaan hebben om mij deze studie tot een goed einde te laten brengen.

Contents

Chapter 1

Introduction

This is a report of the study done as an undergraduate student in Computational Chemistry, and will cover the theory and results of quantum mechanical calculations on HX (X $=$ Cl, F) dimers. HX dimers are Van der Waals complexes, consisting of two HX molecules. The molecules are held together by a hydrogen bond, which is a relatively strong Van der Waals force. Figure 1.1 shows such a complex, together with its internal coordinates.

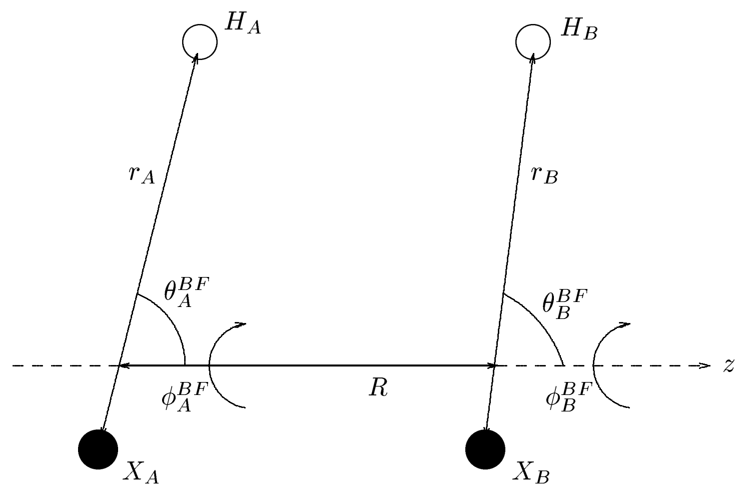

Figure 1.1: Overview of an $(HX)_2$ van der Waals system, with internal coordinates $(r_A, r_B, R, \theta_A^{BF}, \phi_A^{BF}, \theta_B^{BF}, \phi_B^{BF})$.

$(HF)_2$ and $(HCl)_2$ are widely studied systems, since they are relatively simple and contain a hydrogen bond. Calculations on the dynamics of such a system comes down to finding eigenvalues and eigenfunctions of the Hamiltonian operator (section 2.2), which consists of a kinetic and a potential part. For the potential part several potential energy surfaces (PES) are used. The kinetic part consists of the vibrational and rotational motions of the molecule, and the interactions between these motions.

Infrared spectrosopy of HX dimers measures transitions between ground state $(HX)_2$ and the excited dimer by excitation of one or more of the intermolecular or intramolecular modes of the dimer. The interpretation of such a spectrum therefore requires knowledge of the energy levels and wave functions of the system in the ground state as well as excited states. In this work the ground state and the states where one of the monomers is vibrationally excited are studied. Since the vibrationally excited energy levels are well above the dissociation limit of the dimer, these states are not really bound states, but rather narrow resonances in the continuum.

Chapter 2

Theory

This chapter describes the theory behind the computation. It starts with an overview of the conventions in this report. Next a derivation of the Hamiltonian for a dimer consisting of two diatomics is given in section 2.2, followed by a description of the basis functions and matrix elements in section 2.3. Finally, section 2.4 deals with the symmetry of the Hamiltonian.

2.1 Conventions

First, the notational conventions have to be defined. Scalars are denoted in italic, vectors in bold face, and the polar angles of a vector in bold face with a hat on top. Hence, a vector $\mathbf{R}$ has length R and polar angles $\hat{\mathbf{R}}$. Operators are denoted by a hat on top of them. The matrix of an operator $\hat{A}$ is written as $\mathbb{A}$.

2.2 The Hamiltonian

The Hamiltonian $\hat{H}$ can be written as the sum of the kinetic energy $\hat{T}$ and the potential V:

$$\hat{H} = \hat{T} + V. \tag{2.1}$$

Each of these terms will be discussed separately: the kinetic energy operator in section 2.2.1 and the potential energy in section 2.2.2.

2.2.1 The kinetic energy

The kinetic energy of a two-particle system is classically given as:

$$T_A^{tot} = \frac{1}{2} m_1 \dot{r}_1^2 + \frac{1}{2} m_2 \dot{r}_2^2, \tag{2.2}$$

where m_1 and m_2 are the masses of atoms 1 and 2, and $\dot{\mathbf{r}}_1$ and $\dot{\mathbf{r}}_2$ are the time derivatives of their positions $\mathbf{r}_1$ and $\mathbf{r}_2$ (see figure 2.1).

We can now define the vectors $\mathbf{r}_A$ as the vector pointing from atom 1 to atom 2, and $\mathbf{R}_A$ as the the center of mass of diatom A:

$$\mathbf{r}_A \equiv \mathbf{r}_2 - \mathbf{r}_1, \tag{2.3}$$

$$\mathbf{R}_A \equiv \frac{1}{m_A}\left(m_1 \mathbf{r}_1 + m_2 \mathbf{r}_2\right), \tag{2.4}$$

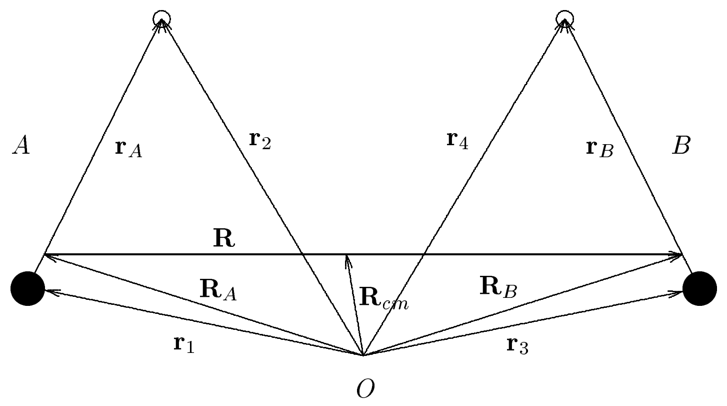

Figure 2.1: Overview of a dimer consisting of two diatomics in a space fixed (SF) frame.

where $m_A = m_1 + m_2$ is the total mass of diatom A. With this, $\mathbf{r}_1$ and $\mathbf{r}_2$ can be rewritten as:

$$\mathbf{r}_1 = \mathbf{R}_A - \frac{m_2}{m_A}\mathbf{r}_A, \tag{2.5}$$

$$\mathbf{r}_2 = \mathbf{R}_A + \frac{m_1}{m_A}\mathbf{r}_A. \tag{2.6}$$

Combining these expressions with Eq. (2.2), the total kinetic energy of diatom A becomes

$$\begin{aligned} T_A^{tot} &= \frac{1}{2}m_1\left(\dot{\mathbf{R}}_A - \frac{m_2}{m_A}\dot{\mathbf{r}}_A\right)^2 + \frac{1}{2}m_2\left(\dot{\mathbf{R}}_A + \frac{m_1}{m_A}\dot{\mathbf{r}}_A\right)^2 \\ &= \frac{1}{2}m_A\dot{R}_A^2 + \frac{1}{2}\frac{m_1m_2}{m_A}\left(\frac{m_2}{m_A} + \frac{m_1}{m_A}\right)\dot{r}_A^2 \\ &= \frac{1}{2}m_A\dot{R}_A^2 + \frac{1}{2}\mu_A\dot{r}_A^2 = \frac{1}{2}m_A\dot{R}_A^2 + \frac{p_A^2}{2\mu_A}. \end{aligned} \tag{2.7}$$

In the resulting expression the term $\frac{1}{2}m_A\dot{R}_A^2$ describes the overall center of mass motion of the diatom while the term $\frac{p_A^2}{2\mu_A}$ defines its rotational and vibrational motions by means of its reduced mass

$$\mu_A = \frac{m_1m_2}{m_1 + m_2} \tag{2.8}$$

and momentum $\mathbf{p}_A = \mu_A\dot{\mathbf{r}}_A$. As $\mathbf{r}_A$ is defined in a Cartesian frame, the quantum mechanical form of the rightmost term in Eq. (2.7) can be obtained by making the replacements $p_{A\alpha} \rightarrow -i\hbar\frac{\partial}{\partial\alpha}$ for $\alpha = x_A, y_A, z_A$. Doing so results in the internal kinetic energy operator for diatom A:

$$\hat{T}_A = -\frac{\hbar^2}{2\mu_A}\left(\frac{\partial^2}{\partial {x_A}^2} + \frac{\partial^2}{\partial {y_A}^2} + \frac{\partial^2}{\partial {z_A}^2}\right) = -\frac{\hbar^2}{2\mu_A}\hat{\nabla}_A^2, \tag{2.9}$$

where $\hat{\boldsymbol{\nabla}}_A = \left(\frac{\partial}{\partial x_A}, \frac{\partial}{\partial y_A}, \frac{\partial}{\partial z_A}\right)$. Using the definition for the space fixed angular momentum operator of a diatomic (see appendix A) this operator becomes

$$\hat{T}_A = -\frac{\hbar^2}{2\mu_A}\frac{1}{r_A^2}\frac{\partial}{\partial r_A}r_A^2\frac{\partial}{\partial r_A} + \frac{\left(\hat{j}_A^{SF}\right)^2}{2\mu_A r_A^2}, \tag{2.10}$$

where $\hat{\mathbf{j}}_A^{SF}$ is the angular momentum operator for diatom A, describing its rotational motions with respect to the space fixed frame. The derivative term in Eq. (2.10) describes its vibrational (stretch) motion. By means of the commutation relation

$$\left[\frac{\partial}{\partial r}, r\right] = \hat{1}, \tag{2.11}$$

we can rewrite this vibrational term to

$$\frac{1}{r_A^2}\frac{\partial}{\partial r_A}r_A^2\frac{\partial}{\partial r_A} = \frac{1}{r_A^2}\left(\hat{1} + r_A\frac{\partial}{\partial r_A}\right)\left(\frac{\partial}{\partial r_A}r_A - \hat{1}\right) = \frac{1}{r_A}\frac{\partial^2}{\partial {r_A}^2}r_A. \tag{2.12}$$

Expression similar to those in Eqs. (2.10) and (2.12) are found for the internal energy operator for diatom B.

The remaining center of mass motions (the time derivative terms in Eq. (2.7) and its counterpart for monomer B) represent the kinetic energy of the dimer. For this kinetic energy we can proceed in a completely analogous way, defining $\mathbf{R}$ and $\mathbf{R}_{cm}$ as

$$\begin{aligned} \mathbf{R} &\equiv \mathbf{R}_B - \mathbf{R}_A, & (2.13)\\ \mathbf{R}_{cm} &\equiv \frac{1}{M}\left(m_A\mathbf{R}_A + m_B\mathbf{R}_B\right) & (2.14) \end{aligned}$$

with $M = m_A + m_B$, rewriting $\mathbf{R}_A$ and $\mathbf{R}_B$ and following Eq. (2.7) we arrive at

$$\begin{aligned} T_{AB}^{tot} &= \frac{1}{2}m_A\dot{R}_A^2 + \frac{1}{2}m_B\dot{R}_B^2 \\ &= \frac{1}{2}M\dot{R}_{cm}^2 + \frac{p_{AB}^2}{2\mu_{AB}}, \end{aligned} \tag{2.15}$$

where $\mathbf{p}_{AB}$ is the momentum of the dimer, and μ_{AB} represents its reduced mass. The first term on the right hand side denotes the translation of the dimer as a whole and the second term the vibrational and rotational internal motions. We can now rewrite this last term in a quantum mechanical form by introducing the (space fixed) end-over-end angular momentum operator $\hat{\mathbf{l}}^{SF}$, which represents the end-over-end rotation of the monomers:

$$\begin{aligned} \hat{T}_{AB} &= \frac{p_{AB}^2}{2\mu_{AB}} \\ &= -\frac{\hbar^2}{2\mu_{AB}}\hat{\nabla}_{AB}^2 \\ &= -\frac{\hbar^2}{2\mu_{AB}}\frac{1}{R}\frac{\partial^2}{\partial R^2}R + \frac{\left(\hat{l}^{SF}\right)^2}{2\mu_{AB}R^2}. \end{aligned} \tag{2.16}$$

As the overall translational energy of the dimer moving in homogeneous space is constant, it only causes a shift in the total energy of the system and we no longer consider it. Hence, we arrive at the kinetic energy operator for a system of two diatomics:

$$\begin{aligned} \hat{T} &= \hat{T}_A + \hat{T}_B + \hat{T}_{AB} \\ &= -\frac{\hbar^2}{2\mu_A}\frac{1}{r_A}\frac{\partial^2}{\partial {r_A}^2}r_A + \frac{\left(\hat{j}_A^{SF}\right)^2}{2\mu_A r_A^2} \end{aligned}$$

$$
\begin{aligned}
&- \frac{\hbar^2}{2\mu_B}\frac{1}{r_B}\frac{\partial^2}{\partial r_B{}^2} r_B + \frac{\left(\hat{j}_B^{SF}\right)^2}{2\mu_B r_B^2} \\
&- \frac{\hbar^2}{2\mu_{AB}}\frac{1}{R}\frac{\partial^2}{\partial R^2} R + \frac{\left(\hat{l}^{SF}\right)^2}{2\mu_{AB} R^2}.
\end{aligned} \tag{2.17}
$$

When changing to body fixed coordinates, the z-axis is laid along $\mathbf{R}$ (see figure 1.1), and hence the representation of $\mathbf{R}$ changes to $\mathbf{R} = (0,0,R)^T$ and $\hat{\mathbf{R}} \equiv (\beta,\alpha) = (0,0)$. Using the expressions in appendix A we see that Eq. (2.17) turns into

$$
\begin{aligned}
\hat{T} \;=\; & -\frac{\hbar^2}{2\mu_A}\frac{1}{r_A}\frac{\partial^2}{\partial r_A{}^2} r_A + \frac{\hat{j}_A^2}{2\mu_A r_A^2} \\
& - \frac{\hbar^2}{2\mu_B}\frac{1}{r_B}\frac{\partial^2}{\partial r_B{}^2} r_B + \frac{\hat{j}_B^2}{2\mu_B r_B^2} \\
& - \frac{\hbar^2}{2\mu_{AB}}\frac{1}{R}\frac{\partial^2}{\partial R^2} R + \frac{\left(\hat{J}^{SF}\right)^2 + \left(\hat{j}\right)^2 - 2\hat{\mathbf{j}}\cdot\hat{\mathbf{J}}}{2\mu_{AB} R^2}.
\end{aligned} \tag{2.18}
$$

In Eq. (2.18) the operators $\hat{\mathbf{j}}_X$ have a space fixed form (see appendix A), but operate on the body fixed angles $(\phi_X^{BF}, \theta_X^{BF})$. $\hat{\mathbf{J}}$ is the total angular momentum with respect to the dimer embedded axes. Since its projections on these axes, $\hat{J}_x$, $\hat{J}_y$, and $\hat{J}_z$, do not satisfy the normal commutation relations [Eq. (A.2)], nor the anomolous ones [Eq. (A.6)], it is often referred to as a pseudo-angular momentum operator. $\hat{\mathbf{J}}^{SF}$ is the total angular momentum with respect to the space fixed axes. The operator $\hat{\mathbf{j}}$ is defined as $\hat{\mathbf{j}} \equiv \hat{\mathbf{j}}_A + \hat{\mathbf{j}}_B$.

The term $2\hat{\mathbf{j}}\cdot\hat{\mathbf{J}}$ is called the Coriolis coupling. This coupling can be rewritten as

$$
2\hat{\mathbf{j}}\cdot\hat{\mathbf{J}} \equiv 2\hat{j}_z\hat{J}_z + \hat{j}_+\hat{J}_+ + \hat{j}_-\hat{J}_-, \tag{2.19}
$$

where the step operators $\hat{j}_\pm$ and $\hat{J}_\pm$ are defined by

$$
\hat{j}_\pm \equiv \hat{j}_x \pm i\hat{j}_y \qquad \text{and} \qquad \hat{J}_\pm \equiv \hat{J}_x \mp i\hat{J}_y. \tag{2.20}
$$

2.2.2 The potential energy

Spherical expansion

In order to be able to compute the matrix elements for the potential energy V, it is expanded in terms of the angular momentum basis functions. In a space fixed frame these angular functions depend on the orientation of vectors $\mathbf{r}_A^{SF}$, $\mathbf{r}_B^{SF}$ and $\mathbf{R}$, and hence we can write the expansion as

$$
V(r_A, r_B, R, \hat{\mathbf{r}}_A^{SF}, \hat{\mathbf{r}}_B^{SF}, \hat{\mathbf{R}}) = \sum_\Lambda v_\Lambda(r_A, r_B, R) A_\Lambda(\hat{\mathbf{r}}_A^{SF}, \hat{\mathbf{r}}_B^{SF}, \hat{\mathbf{R}}), \tag{2.21}
$$

where $\Lambda \equiv (L_A, L_B, L)$ labels the angular basis functions, which are given by

$$
\begin{aligned}
A_\Lambda(\hat{\mathbf{r}}_A^{SF}, \hat{\mathbf{r}}_B^{SF}, \hat{\mathbf{R}}) \;=\; & \sum_{M_A, M_B, M} (-1)^{L_A+L_B+L} \begin{pmatrix} L_A & L_B & L \\ M_A & M_B & M \end{pmatrix} \times \\
& C_{M_A}^{L_A}(\hat{\mathbf{r}}_A^{SF}) C_{M_B}^{L_B}(\hat{\mathbf{r}}_B^{SF}) C_M^L(\hat{\mathbf{R}}).
\end{aligned} \tag{2.22}
$$

Here, the expression in large parentheses is a Wigner 3-j symbol, and the $C_m^{(l)}$ are spherical harmonics in Racah normalization:

$$C_m^l(\beta,\alpha) = \sqrt{\frac{4\pi}{2l+1}} Y_m^l(\beta,\alpha). \tag{2.23}$$

When doing the expansion in body fixed coordinates we make use of the fact that the angular basis functions are invariant to any frame rotation. Furthermore, in the body fixed frame $\hat{\mathbf{R}} = (0,0)$, and hence $C_M^L(\hat{\mathbf{R}}) = C_M^L(0,0) = \delta_{M0}$. Using the property of 3-j symbols that $M_A + M_B + M = 0$, we get

$$A_\Lambda(\hat{\mathbf{r}}_A^{BF}, \hat{\mathbf{r}}_B^{BF}) = \sum_{M_A} (-1)^{L_A+L_B+L} \begin{pmatrix} L_A & L_B & L \\ M_A & -M_A & 0 \end{pmatrix} C_{M_A}^{L_A}(\hat{\mathbf{r}}_A^{BF}) C_{-M_A}^{L_B}(\hat{\mathbf{r}}_B^{BF}). \tag{2.24}$$

Since the angular functions are orthogonal, the expansion coefficients v_Λ can be written as

$$\begin{aligned} v_\Lambda(r_A, r_B, R) &= \frac{\langle A_\Lambda | V \rangle}{\langle A_\Lambda | A_\Lambda \rangle} \\ &= \frac{(2L_A+1)(2L_B+1)(2L+1)}{16\pi^2} \times \\ & \quad \int \mathrm{d}\hat{\mathbf{r}}_A \int \mathrm{d}\hat{\mathbf{r}}_B A_\Lambda(\hat{\mathbf{r}}_A, \hat{\mathbf{r}}_B)^* V(r_A, r_B, R, \hat{\mathbf{r}}_A, \hat{\mathbf{r}}_B), \end{aligned} \tag{2.25}$$

where $\mathrm{d}\hat{\mathbf{r}}_X = \sin\theta_X \mathrm{d}\phi_X \mathrm{d}\theta_X$. In practice the BF frame is chosen in such a way that one of the Euler angles ϕ_A or ϕ_B is zero and can be omitted from the integration. The above integration can be performed for each (r_A, r_B, R) combination, thus defining the expansion coefficients for the potential in a BF as well as a SF frame.

Potential energy surfaces

In this work, several potential energy surfaces are used. A potential energy surface (PES) is important in that it describes many of the characteristics of the system studied. The first surface is $ES1$ PES for the HCl dimer, by Elrod and Saykally [15]. This potential describes the ground state fairly well, but fails to describe the tunneling splittings in the vibrationally excited $(HCl)_2$. Therefore, Qiu, Zhang and Bačić [6] have added an electrostatic interaction potential to this surface, resulting in the $ES1$–EL PES.

For the HF dimer also two surfaces were studied. The first was the $SQSBDE$ PES by Quack and Suhm [16]. This is a PES often studied, and it describes the ground state as well as the excited state quite well. Also, a new surface, the SO–3 PES by Klopper, Quack and Suhm [17] was used.

Damping the potential

On the $(HF)_2$ potentials $SQSBDE$ and SO–3 very high peaks in the potential for certain configurations caused problems in the expansion. This was due to the fact that the integration of Eq. (2.25) was done on a quadrature grid, so that the resulting expansion coefficients did describe the points on the grid, but failed to approximate the potential between these points. Therefore, the potential was damped if it grew too high. This was done by keeping the potential if it were lower than or equal to a certain value V_0, and damping it by means of a tanh function up to a value V_{max} otherwise:

$$\tilde{V} = \begin{cases} V & , \quad V \leq V_0 \\ V_0 + \frac{\tanh[\beta(V-V_0)]}{\beta} & , \quad V > V_0 \end{cases} , \tag{2.26}$$

where the parameter β was defined as $\beta = (V_{max} - V_0)^{-1}$. Using this function assures that the $\tilde{V}$ is continuous around V_0 up to the second derivative in V.

2.3 Basis functions and matrix elements

The eigenfunctions of the derived Hamiltonian are computed using the variation principle as an expansion in a certain basis. They can be found by diagonalization of the matrix of the Hamiltonian in this basis. The basis functions used are explained in section 2.3.1 whereas the matrix elements of the Hamiltonian are dealt with in section 2.3.2.

2.3.1 Basis functions

For the angular basis the complex conjugates of Wigner rotation functions, $D^{(j)*}_{mk}$, are used. These functions are eigenfunctions of the symmetric top Hamiltonian, since

$$\begin{aligned} \hat{j}_z^{SF} D^{(j)}_{mk}(\alpha,\beta,\gamma)^* &= \hbar m D^{(j)}_{mk}(\alpha,\beta,\gamma)^* \\ \hat{j}_z^{BF} D^{(j)}_{mk}(\alpha,\beta,\gamma)^* &= \hbar k D^{(j)}_{mk}(\alpha,\beta,\gamma)^* \\ (\hat{j}^{SF})^2 D^{(j)}_{mk}(\alpha,\beta,\gamma)^* = (\hat{j}^{BF})^2 D^{(j)}_{mk}(\alpha,\beta,\gamma)^* &= \hbar^2 j(j+1) D^{(j)}_{mk}(\alpha,\beta,\gamma)^* . \end{aligned} \tag{2.27}$$

This is why they are often referred to as symmetric top functions. In [1] it is shown that the set of functions

$$D^{(J)}_{MK}(\alpha,\beta,0)^* \sum_{m_A,m_B} \langle jK |\, j_A m_A; j_B m_B \rangle D^{(j_A)}_{m_A k_A}(\hat{\mathbf{r}}_A)^* D^{(j_B)}_{m_B k_B}(\hat{\mathbf{r}}_B)^* \tag{2.28}$$

forms a suitable angular basis with respect to a BF frame for an arbitrary system of two rotors. The symbol in brackets is a Clebsch-Gordan coefficient, which gives the transformation between the two orthonormal bases $|\, jK\rangle$ and $|\, j_A m_A; j_B m_B\rangle \equiv |\, j_A m_A\rangle \otimes |\, j_B m_B\rangle$. Clebsch-Gordan coefficients are related to 3-j symbols as

$$\begin{pmatrix} j_1 & j_2 & j_3 \\ m_1 & m_2 & m_3 \end{pmatrix} \equiv \frac{(-1)^{j_1-j_2-m_3}}{\sqrt{2j_3+1}} \langle\, j_3, -m_3 |\, j_1 m_1; j_2 m_2 \rangle. \tag{2.29}$$

Since both monomers are linear in HX dimers $k_A = k_B = 0$, and thus we can replace $D^{(j_X)}_{m_X k_X}(\hat{\mathbf{r}}_X)^*$ by Racah normalized spherical harmonics $C^{(j_X)}_{m_X}(\hat{\mathbf{r}}_X)$, giving

$$D^{(J)}_{MK}(\alpha,\beta,0)^* \sum_{m_A,m_B} \langle jK |\, j_A m_A; j_B m_B \rangle C^{(j_A)}_{m_A}(\hat{\mathbf{r}}_A) C^{(j_B)}_{m_B}(\hat{\mathbf{r}}_B). \tag{2.30}$$

For the monomer radial basis the functions $\chi_X(r_X) \equiv \tilde{\chi}_X(r_X)/r_X$ were used, where the $\tilde{\chi}_X$ are eigenfunctions of the diatomic Hamiltonian

$$\hat{h}^{(mon)}_X(r_X) = -\frac{\hbar^2}{2\mu_X} \frac{\partial^2}{\partial {r_X}^2} + V^{(mon)}_X(r_X). \tag{2.31}$$

Similarly, the dimer stretch basis functions are $\varphi(R) \equiv \tilde{\varphi}(R)/R$, where the $\tilde{\varphi}$ are obtained from the reference hamiltonian

$$\hat{h}^{(dim)} = -\frac{\hbar^2}{2\mu_{AB}} \frac{\partial^2}{\partial R^2} + V^{(dim)}(R). \tag{2.32}$$

The eigenfunctions were calculated using a discrete variable representation (DVR). A DVR (for $r = r_A, r_B, R$) consists of an orthonormal basis set

$$\{\phi_i(r),\ i = 0, \ldots, n_r - 1\} \tag{2.33}$$

and an n_r-point quadrature with the points and weights

$$\{(r_k, w_k),\ k = 0, \ldots, n_r - 1\} \tag{2.34}$$

with the property

$$\phi_i(r_k) = w_k^{-\frac{1}{2}} \delta_{ik}. \tag{2.35}$$

For this problem, a sinc-function DVR [2] was used, with basis functions

$$\phi_i(r) = \Delta_r^{-\frac{1}{2}} \operatorname{sinc}\left[\pi\left(\frac{r - r_0}{\Delta_r} - i\right)\right],\ i = 0, \ldots, n_r - 1, \tag{2.36}$$

where $\operatorname{sinc}(r) \equiv \frac{\sin(r)}{r}$ and Δ_r is the distance between two grid points. The quadrature corresponding to this basis is $\{(r_k, w_k) = (r_0 + k\Delta_r, \Delta_r),\ k = 0, \ldots, n_r - 1\}$.

In any DVR, the potential is diagonal, since

$$\begin{aligned} \mathbb{V}_{ij} &= \langle \phi_i \,|\, V \,|\, \phi_j \rangle \\ &\approx \sum_{k=0}^{n_r - 1} w_k \phi_i(r_k)^* V(r_k) \phi_j(r_k) \\ &= \sum_{k=0}^{n_r - 1} \delta_{ik} V(r_k) \delta_{jk} \\ &= V(r_i)\delta_{ij}. \end{aligned} \tag{2.37}$$

For the sinc-DVR, the second derivative terms are given in [2] as

$$\langle \phi_i \,|\, \frac{\partial^2}{\partial r^2} \,|\, \phi_j \rangle = \begin{cases} -\frac{\pi^2}{3\Delta_r^2} & , \quad i = j \\ -\frac{2(-1)^{i-j}}{(i-j)^2 \Delta_r^2} & , \quad i \neq j \end{cases}. \tag{2.38}$$

The monomer reference Hamiltonian matrices $\mathbb{H}_X^{(mon)}$ thus consist of elements

$$\begin{aligned} \mathbb{H}_{X,ij}^{(mon)} &= \langle \phi_i \,|\, \hat{h}_X^{(mon)} \,|\, \phi_j \rangle \\ &= \begin{cases} \frac{\hbar^2 \pi^2}{6\mu_X \Delta_{r_X}^2} + V_X^{(mon)}(r_{X,i}) & , \quad i = j \\ \frac{\hbar^2 (-1)^{i-j}}{\mu_X (i-j)^2 \Delta_{r_X}^2} & , \quad i \neq j \end{cases}. \end{aligned} \tag{2.39}$$

Diagonalization of this matrix results in a set of diatomic vibration functions $\{\tilde{\chi}_{X,i}(r_X)\}$ with associated energies $\{E_{X,i}^{(mon)}\}$. Dividing these eigenfunctions by the stretch coordinate r_X then gives the basis functions for the Hamiltonian.

Calculations were done with two different monomer reference potentials. The first was the potential of the free monomer, which was obtained by making a cut through the potential surface at very large value of R. The functions resulting from this potential will be called $\{\chi_{X,i}^{(inf)}(r_X)\}$; the energies $\{E_{X,i}^{(mon,inf)}\}$. The second potential was obtained by minimization of the potential around the equilibrium while keeping the r_X fixed at the points on the grid. To preserve $PI(C_{2v})$ symmetry in the basis, the mean of the the minimum potentials for diatom A and B was used for both diatoms:

$$V_A^{(eq)} = V_B^{(eq)} = \frac{V_A^{min} + V_B^{min}}{2}. \tag{2.40}$$

This potential resulted in the set of vibration functions $\{\chi_{X,i}^{(eq)}(r_X)\}$ and energies $\{E_{X,i}^{(mon,eq)}\}$.

Since the monomers are equal $V_A^{(inf)}$ and $V_B^{(inf)}$ are equal, and thus the corresponding sets $\{\chi_{A,i}^{(inf)}\}$ and $\{\chi_{B,i}^{inf}\}$ will also be the same. By definition, $V_A^{(eq)}$ and $V_B^{(eq)}$ are also the same, resulting in the same sets $\{\chi_{A,i}^{(eq)}\}$ and $\{\chi_{B,i}^{(eq)}\}$. For this reason we will drop the X label on the monomer functions and energies.

The reference potential for the dimer vibration, $V^{(dim)}(R)$, is obtained by minimizing the potential in the monomer stretch coordinates, while keeping the intermolecular distance fixed on the grid $\{R_i\}$ and the angular coordinates at their equilibrium values in the dimer. Diagonalization of the reference Hamiltonian $\mathbb{H}^{(dim)}$ [Eq. (2.39) with μ_X, r_X and $V_X^{(mon)}$ replaced by μ_{AB}, R and $V^{(dim)}$] and dividing the eigenfunctions by R gives the set of dimer vibration functions $\{\varphi_i(R)\}$ and energies $\{E_i^{(dim)}\}$.

The total normalized basis functions for the HX dimers are then given by

$$\begin{aligned} & |\, v_A, v_B, v_{AB}, j_A, j_B, j, K; J, M\rangle \\ = \quad & \chi_{v_A}(r_A)\chi_{v_B}(r_B)\varphi_{v_{AB}}(R)\sqrt{\frac{(2j_A+1)(2j_B+1)(2J+1)}{64\pi^3}} D_{MK}^{(J)}(\alpha,\beta,0)^* \times \\ & \sum_{m_A,m_B} \langle jK|\, j_A m_A; j_B m_B\rangle C_{m_A}^{j_A}(\theta_A^{BF},\phi_A^{BF}) C_{m_B}^{j_B}(\theta_B^{BF},\phi_B^{BF}), \end{aligned} \tag{2.41}$$

where χ_{v_X} is $\chi_{v_X}^{(inf)}$ or $\chi_{v_X}^{(eq)}$.

2.3.2 Matrix elements

As now both the Hamiltonian operator $\hat{H}$ and the basis are defined we can now construct the Hamiltonian matrix $\mathbb{H}$ by calculating the matrix elements $\mathbb{H}_{ij} \equiv \langle i\,|\,\hat{H}\,|\,j\rangle$. The matrix elements resulting from the kinetic energy operator will be discussed first, and after that the potential energy matrix elements are defined.

Kinetic energy matrix elements

Before giving the matrix elements for the full Hamiltonian we derive for the monomer stretch integrals that

$$
\begin{aligned}
& \langle v'_X \,|\, -\frac{\hbar^2}{2\mu_X}\frac{1}{r_X}\frac{\partial^2}{\partial {r_X}^2} r_X \,|\, v_X \rangle \\
= \;& -\frac{\hbar^2}{2\mu_X}\int r_X^2 \chi_{v'_X}(r_X)^* \frac{1}{r_X}\frac{\partial^2}{\partial {r_X}^2} r_X \chi_{v_X}(r_X) \mathrm{d}r_X \\
= \;& -\frac{\hbar^2}{2\mu_X}\int r_X \frac{\tilde{\chi}_{v'_X}(r_X)^*}{r_X}\frac{\partial^2}{\partial {r_X}^2} r_X \frac{\tilde{\chi}_{v_X}(r_X)}{r_X} \mathrm{d}r_X \\
= \;& -\frac{\hbar^2}{2\mu_X}\int \tilde{\chi}_{v'_X}(r_X)^* \frac{\partial^2}{\partial {r_X}^2} \tilde{\chi}_{v_X}(r_X) \mathrm{d}r_X \\
= \;& \int \tilde{\chi}_{v'_X}(r_X)^* \left(-\frac{\hbar^2}{2\mu_X}\frac{\partial^2}{\partial {r_X}^2} + V_X^{(mon)}(r_X)\right) \tilde{\chi}_{v_X}(r_X) \mathrm{d}r_X \\
& - \int \tilde{\chi}_{v'_X}(r_X)^* V_X^{(mon)}(r_X) \tilde{\chi}_{v_X}(r_X) \mathrm{d}r_X \\
= \;& E_{v_X}^{(mon)} \delta_{v'_X v_X} - \int r_X^2 \frac{\tilde{\chi}_{v'_X}(r_X)}{r_X}^* V_X^{(mon)}(r_X) \frac{\tilde{\chi}_{v_X}(r_X)}{r_X} \mathrm{d}r_X \\
= \;& E_{v_X}^{(mon)} \delta_{v'_X v_X} - \langle v'_X \,|\, V_X^{(mon)} \,|\, v_X \rangle,
\end{aligned}
\tag{2.42}
$$

where the extra r_X^2 term in the integral arises from the volume element in spherical coordinates $r_X^2 \sin\theta_X \mathrm{d}r_X \mathrm{d}\theta_X \mathrm{d}\phi_X$. Similarly, the dimer stretch integrals are

$$
\langle v'_{AB} \,|\, -\frac{\hbar^2}{2\mu_{AB}}\frac{1}{R}\frac{\partial^2}{\partial R^2} R \,|\, v_{AB} \rangle = E_{v_{AB}}^{(dim)} \delta_{v'_{AB} v_{AB}} - \langle v'_{AB} \,|\, V^{(dim)} \,|\, v_{AB} \rangle. \tag{2.43}
$$

Hence, by subtracting the reference potentials from the full potential the matrix elements for the stretch motions are easily calculated.

The matrix elements for the total kinetic energy can then be found by applying the kinetic energy operator from Eq. (2.18) on the basis functions of Eq. (2.41), using the expressions of Eqs. (2.27), (2.42) and (2.43):

$$
\begin{aligned}
& \langle v'_A, v'_B, v'_{AB}, j'_A, j'_B, j', K'; J, M \,|\, \hat{T} \,|\, v_A, v_B, v_{AB}, j_A, j_B, j, K; J, M \rangle \\
= \;& \Bigg\{ \left[E_{v_A}^{(mon)} + E_{v_B}^{(mon)} + E_{v_{AB}}^{(dim)} \right] \delta_{v'_A v_A} \delta_{v'_B v_B} \delta_{v'_{AB} v_{AB}} \delta_{K' K} \\
& + \Big[\frac{\hbar^2}{2\mu_A} \langle v'_A \,|\, \frac{1}{r_A^2} \,|\, v_A \rangle j_A (j_A + 1) \delta_{v'_B v_B} \\
& + \frac{\hbar^2}{2\mu_B} \langle v'_B \,|\, \frac{1}{r_B^2} \,|\, v_B \rangle j_B (j_B + 1) \delta_{v'_A v_A} \Big] \delta_{v'_{AB} v_{AB}} \delta_{K' K} \\
& + \frac{\hbar^2}{2\mu_{AB}} \langle v'_{AB} \,|\, \frac{1}{R^2} \,|\, v_{AB} \rangle \Big[\left[J(J+1) + j(j+1) - 2K^2 \right] \delta_{K' K} \\
& - \left[C_{jK}^{+} C_{JK}^{+} \delta_{K', K+1} + C_{jK}^{-} C_{JK}^{-} \delta_{K', K-1} \right] \Big] \delta_{v'_A v_A} \delta_{v'_B v_B} \\
& \Bigg\} \delta_{j'_A j_A} \delta_{j'_B j_B} \delta_{j' j},
\end{aligned}
\tag{2.44}
$$

where we must take care that the reference potentials used in the calculations of the vibrational basis functions are subtracted from the total potential. The rotational constants matrix elements $\langle v'_X \,|\, r_X^{-2} \,|\, v_X \rangle$ can be evaluated on the quadrature grid $\{r_i\}$ by

$$
\langle v'_X \,|\, \frac{1}{r_X^2} \,|\, v_X \rangle = \sum_i \tilde{\chi}_{v'_X}(r_i) \frac{1}{r_i^2} \tilde{\chi}_{v_X}(r_i), \tag{2.45}
$$

since the volume element $r_X^2 \mathrm{d}r_X$ commutes with the operator r^{-2}. The same reasoning holds for the $\langle\, v'_{AB} \,|\, R^{-2} \,|\, v_{AB} \rangle$ elements. The off-diagonal Coriolis terms $C^{\pm}_{lK}$, which arise from the last two terms in Eq. (2.19) couple basis functions with $\Delta K = \pm 1$, and are given by

$$C^{\pm}_{lK} = \sqrt{l(l+1) - K(K \pm 1)}. \tag{2.46}$$

Potential energy matrix elements

The matrix elements for the potential energy can be found in [1]. Adapting the expression given there by setting K_A, K_B, k_A and k_B to zero, and including the phase factor $(-1)^{L_A+L_B+L}$ and the integral of the expansion coefficients over r_A and r_B gives us

$$\begin{aligned}
& \langle\, v'_A, v'_B, v'_{AB}, j'_A, j'_B, j', K'; J, M \,|\, V \,|\, v_A, v_B, v_{AB}, j_A, j_B, j, K; J, M \rangle \\
= \; & \delta_{K'K} \sum_{L_A, L_B, L} \langle\, v'_A, v'_B, v'_{AB} \,|\, v_{L_A L_B L} \,|\, v_A, v_B, v_{AB} \rangle (-1)^{j_A+j_B+j+L_A+L_B-K} \\
& \times [(2j'_A+1)(2j_A+1)(2j'_B+1)(2j_B+1)(2j'+1)(2j+1)]^{\frac{1}{2}} \\
& \times \begin{pmatrix} j'_A & L_A & j_A \\ 0 & 0 & 0 \end{pmatrix} \begin{pmatrix} j'_B & L_B & j_B \\ 0 & 0 & 0 \end{pmatrix} \begin{pmatrix} j' & L & j \\ -K & 0 & K \end{pmatrix} \\
& \times \begin{Bmatrix} j'_A & L_A & j_A \\ j'_B & L_B & j_B \\ j' & L & j \end{Bmatrix}.
\end{aligned} \tag{2.47}$$

In this expression the symbol between braces is a Wigner 9-j symbol. Because the volume element $r_A^2 r_B^2 R^2 \mathrm{d}r_A \mathrm{d}r_B \mathrm{d}R$ commutes with the expansion coefficients, the matrix elements $\langle\, v'_A, v'_B, v'_{AB} \,|\, v_{L_A L_B L} \,|\, v_A, v_B, v_{AB} \rangle$ can be calculated with the $\tilde{\chi}_X$ and $\tilde{\varphi}$ functions by using the quadrature on the discrete r_X and R grids:

$$\begin{aligned}
& \langle\, v'_A, v'_B, v'_{AB} \,|\, v_{L_A L_B L} \,|\, v_A, v_B, v_{AB} \rangle \\
= \; & \sum_{i,j,k} \tilde{\chi}_{v'_A}(r_i) \tilde{\chi}_{v'_B}(r_j) \tilde{\varphi}_{v'_{AB}}(R_k) v_{L_A, L_B, L}(r_i, r_j, R_k) \tilde{\chi}_{v_A}(r_i) \tilde{\chi}_{v_B}(r_j) \tilde{\varphi}_{v_{AB}}(R_k).
\end{aligned} \tag{2.48}$$

2.4 Symmetry

In principle, the eigenvalues of the Hamiltonian can now be found by diagonalization of the matrix defined in section 2.3.2 for a large enough basis. In order to reduce the computational effort we use a symmetry adapted basis. In this basis, the Hamiltonian matrix has a block-diagonal form (figure 2.2). These blocks can be diagonalized separately, thereby greatly reducing the computation time. Doing so also allows one to diagonalize the blocks simultaneously, using multiple processors.

For a complete description of the symmetry of a molecule one would have to look at the group consisting of all permutations of identical nuclei, space inversion, and all products of permutations and inversion. In practice however, only the so-called feasible permutation-inversions are considered, i.e. only the operations that are physically meaningful in the sense that they give rise to observable splittings

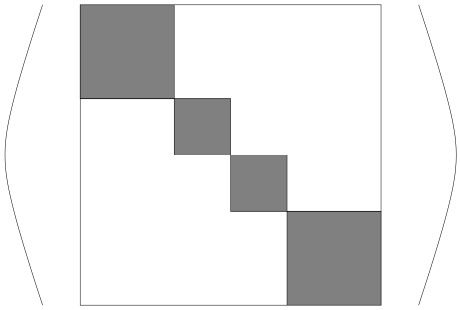

Figure 2.2: Sketch of a block-diagonal matrix. Only the elements in grey are non-zero.

in the spectrum. This group is called the molecular symmetry (MS) group [18], and can be orders of magnitude smaller than the full permutation-inversion group. The MS group of the HX dimer is $\{\hat{E}, \hat{P}\} \otimes \{\hat{E}, \hat{E}^*\}$. The operators are $\hat{E}$, the

PI	r_A	θ_A	ϕ_A	r_B	θ_B	ϕ_B	β	α
$\hat{E}$	r_A	θ_A	ϕ_A	r_B	θ_B	ϕ_B	β	α
$\hat{P}$	r_B	$\pi-\theta_B$	$-\phi_B$	r_A	$\pi-\theta_A$	$-\phi_A$	$\pi-\beta$	$\pi+\alpha$
$\hat{E}^*$	r_A	θ_A	$\pi-\phi_A$	r_B	θ_B	$\pi-\phi_B$	$\pi-\beta$	$\pi+\alpha$
$\hat{P}^*$	r_B	$\pi-\theta_B$	$\pi+\phi_B$	r_A	$\pi-\theta_A$	$\pi+\phi_A$	β	α

Table 2.1: Effect of the elements of $PI(C_{2v})$ on the coordinates of $(HX)_2$.

unity operator which leaves the system unchanged, $\hat{P}$, the permutation operator that exchanges the monomers, and $\hat{E}^*$, the space inversion operator. The product $\hat{P}\hat{E}^* = \hat{E}^*\hat{P}$ will be denoted $\hat{P}^*$. All operators leave R unchanged. The effects on r_A, r_B, $\hat{\mathbf{r}}_A$, $\hat{\mathbf{r}}_B$ and $\hat{\mathbf{R}}$ are derived in appendix B, and the results are displayed in table 2.1. The effects of the operators on the basis functions are derived in appendix C and the results are given in table 2.2.

PI		$\lvert v_A, v_B\rangle$	$\lvert v_{AB}\rangle$	$\lvert j_A, j_B, j, K; J, M\rangle$
$\hat{E}$		$\lvert v_A, v_B\rangle$	$\lvert v_{AB}\rangle$	$\lvert j_A, j_B, j, K; J, M\rangle$
$\hat{P}$	$(-1)^{j_A+j_B+J}$	$\lvert v_B, v_A\rangle$	$\lvert v_{AB}\rangle$	$\lvert j_B, j_A, j, -K; J, M\rangle$
$\hat{E}^*$	$(-1)^{j_A+j_B+j+J}$	$\lvert v_A, v_B\rangle$	$\lvert v_{AB}\rangle$	$\lvert j_A, j_B, j, -K; J, M\rangle$
$\hat{P}^*$	$(-1)^j$	$\lvert v_B, v_A\rangle$	$\lvert v_{AB}\rangle$	$\lvert j_B, j_A, j, K; J, M\rangle$

Table 2.2: Effect of the elements of $PI(C_{2v})$ on the dimer basis functions.

The MS group is isomorphic with the point group C_{2v} and will therefore be denoted by $PI(C_{2v})$. The character table is displayed in table 2.3. Applying the projection operator $\hat{\mathcal{P}}^\Gamma$, defined as

$$\hat{\mathcal{P}}^\Gamma = \frac{1}{4}\left(\hat{E} \pm \hat{P}\right)\left(\hat{E} \pm \hat{E}^*\right) \tag{2.49}$$

	$\hat{E}$	$\hat{P}$	$\hat{E}^*$	$\hat{P}^*$
A_1	1	1	1	1
B_1	1	-1	-1	1
A_2	1	1	-1	-1
B_2	1	-1	1	-1

Table 2.3: Character table of $PI(C_{2v})$. $\hat{E}$ is the unity operator, $\hat{P}$ the permutation operator, $\hat{E}^*$ the space inversion operator and $\hat{P}^*$ the product $\hat{P}\hat{E}^* = \hat{E}^*\hat{P}$.

on a dimer basis function results in a symmetry-adapted basis function, belonging to the Γ irrep. Γ is defined by the two $\pm$ signs in Eq. (2.49. If the first sign is a $+$ then Γ is an A irrep, otherwise a B. If the second sign is equal to the first a subscript 1 is added, otherwise a 2. By describing the Hamiltonian in the symmetry adapted basis it blocks into four blocks on the diagonal, one for each irrep.

Chapter 3

Computational details

3.1 Diagonalization of the Hamiltonian

Since the Hamiltonian matrix becomes very large for large basis sets, diagonalization was not done directly. For the ground state of both dimers the Davidson algorithm was used. In this iterative algorithm the Hamiltonian is implemented as a subroutine that computes its effect on a vector. The Davidson algorithm approximates the i-th eigenvalue λ_i of the Hamiltonian $\hat{H}$ with matrix $\mathbb{H}$ in a certain basis as follows:

1. Choose an orthonormal basis $\mathbb{Q}^{(m)}$ for an m-dimensional subspace of the original problem, with $m \geq i$.
2. Project $\mathbb{H}$ onto the subspace:
$$\tilde{\mathbb{H}} = \mathbb{Q}^T \mathbb{H} \mathbb{Q}. \tag{3.1}$$
3. Solve the subspace problem
$$\tilde{\mathbb{H}} \tilde{\mathbf{x}}_i = \epsilon_i \tilde{\mathbf{x}}_i. \tag{3.2}$$
4. Transform $\tilde{\mathbf{x}}_i$ back to the original basis:
$$\mathbf{x}_i = \mathbb{Q} \tilde{\mathbf{x}}_i. \tag{3.3}$$
5. Compute the residual vector
$$\mathbf{r}_i = (\mathbb{H} - \epsilon_i \mathbb{I}) \mathbf{x}_i. \tag{3.4}$$
6. If $r_i = ||\mathbf{r}_i||$ is less then a predefined maximum error r^{max} accept ϵ_i and $\mathbf{x}_i$ as estimates for λ_i and the associated eigenvector, else
7. Compute the vector
$$\mathbf{q}_i = (\mathbb{D} - \epsilon_i \mathbb{I})^{-1} \mathbf{r}_i, \tag{3.5}$$
where $\mathbb{D}_{ij} = \delta_{ij} \mathbb{H}_{ij}$, and orthogonalize it against $\mathbb{Q}$ (using a Gram-Schmidt process).

8. Add $\mathbf{q}_i$ to $\mathbb{Q}$ resulting in an $(m+1)$-dimensional basis $\mathbb{Q}^{(m+1)}$.

9. Return to step 2 with the new basis.

It may seem that the whole $\mathbb{H}$ matrix is still required for this algorithm, however $\mathbb{HQ}$ in step 2 can be computed by using the subroutine on each of the vectors in $\mathbb{Q}$, step 5 can be done by using it on $\mathbf{x}_i$, and step 7 requires only the diagonal of $\mathbb{H}$ to be known.

The length of the residual vector $\mathbf{r}_i$ gives an upper bound for the error in the computed eigenvalue. This can be shown by writing $\mathbf{x}_i$ in terms of eigenfunctions $\{\mathbf{u}_j\}$ of the Hamiltonian. Defining the vector $\mathbf{y}$ by $y_j = \mathbf{u}_j^T \mathbf{x}_i$, and assuming $\mathbf{x}_i$ to be normalized and the $\mathbf{u}_j$ to be orthonormal, we can write

$$\begin{aligned} r_i = ||\mathbf{r}_i|| = ||(\mathbb{H} - \epsilon_i \mathbb{I})\mathbf{x}_i|| &= ||(\mathbb{H} - \epsilon_i \mathbb{I}) \sum_j y_j \mathbf{u}_j|| \\ &= ||\sum_j y_j(\lambda_j - \epsilon_i)\mathbf{u}_j|| \\ &= \sqrt{\sum_j y_j^2 (\lambda_j - \epsilon_i)^2} \\ &\geq \sqrt{\sum_j y_j^2 \min_k [(\lambda_k - \epsilon_i)^2]} \\ &= \min_k |\lambda_k - \epsilon_i|. \end{aligned} \tag{3.6}$$

Hence, by demanding that $r_i < r^{max}$ it is assured that there exists an eigenvalue between $\epsilon_i - r^{max}$ and $\epsilon_i + r^{max}$. In practice, the eigenvalues are far better converged then r^{max} however.

The Davidson approach was not possible for the vibrationally excited states, since the algorithm converges from the lowest states on, and the excited states are somewhere in the middle of the spectrum. Therefore the excited states are calculated in the following way:

1. The Hamiltonian is calculated in the full primitive basis, and stored to disk.

2. The blocks in the Hamiltonian for which the monomer vibration functions in bra and ket are equal are diagonalized, i.e. for each monomer vibration function a set of eigenfunctions is calculated.

3. Part of these eigenfunctions are used as a new contracted basis. By choosing appropriate eigenfunctions of the uncoupled monomer Hamiltonians, a projection of the Hamiltonian can be made that is small enough to be diagonalized directly, and which still gives a good approximation of the eigenvalues and eigenvectors of the Hamiltonian in the full basis.

Here, the residual vector of an eigenvector $\mathbf{x}_i$ of the Hamiltonian in the contracted basis can be calculated by transforming the vector to the full basis, and applying Eq. (3.4) on the transformed vector.

3.2 Expansion of the potential

The potential was expanded in in angular functions [see Eq. (2.21)] up to $L_A^{max} = L_B^{max} = 11$. In the case of HF dimers it was also damped, using Eq. (2.26) with

$V_0 = 140000\text{cm}^{-1}$ and $V_{max} = 2V_0$. Integration over the angular coordinates was done using a Gauss-Legendre quadrature with 12 points for θ_X and a Gauss-Chebyschev quadrature with also 12 points for ϕ_X.

3.3 The basis

In table 3.1 the ranges and sizes of the radial grids used in the computations are given. The values are chosen in such a way that the stretch basis functions are zero outside the range given and that the DVR (section 2.3.1) has enough grid points to give an accurate description of these functions.

PES		range(R)	n_R	range(r_X)	n_{r_X}
$ES1$	[15]	6.0 – 11.0	35	1.6 – 3.7	23
$ES1–EL$	[6]	6.0 – 11.0	35	1.6 – 3.7	23
$SQSBDE$	[16]	4.0 – 8.0	42	1.0 – 2.9	20
$SO–3$	[17]	4.0 – 8.0	42	1.0 – 3.1	22

Table 3.1: Ranges and number of points of the radial grids used in the calculation of the eigenstates of HX dimers, for various potential surfaces. $ES1$ and $ES1-EL$ are $(HCl)_2$ surfaces, $SQSBDE$ and $SO-3$ are $(HF)_2$ potentials. The ranges are given in bohr (a_0).

In the calculations on $(HCl)_2$, dimer vibrational basis functions were used up to $v_{AB}^{max} = 8$, while for the $(HF)_2$ calculations $v_{AB}^{max} = 6$. The monomer radial basis consisted of the set of functions $\{|\,00\rangle, |\,01\rangle, |\,10\rangle, |\,02\rangle, |\,20\rangle, |\,11\rangle\}$. All calculations where done with $j_A^{max} = j_B^{max} = 11$, and $J = |K| = 0$. In the ground state calculations a value of $r^{max} = 0.1\text{cm}^{-1}$ was used.

In the calculations on the vibrationally excited states a number of the first eigenvectors of the primitive Hamiltonians was taken into the contracted basis for each symmetry adapted monomer vibrational function. This number was expressed as a fraction of the dimension of the primitive basis for the vibrational function. Furthermore, the eigenvectors of the $|\,00\rangle$ Hamiltonian with associated energies (with respect to the ground state of the irrep concerned) between fixed values E^{min} and E^{max} were added to the basis, to take the resonance of the ground state functions with an energy around the vibrational excitation energy with the lower excited functions into account. The fractions and energy boundaries were obtained by studying the Hamiltonian matrix in a small rotational basis ($j_A^{max} = j_B^{max} = 7$), and are given in table 3.2 for each of the PESs studied.

Applying the settings from table 3.2 leads to contracted basis sizes between 3600 and 6000 for the $ES1–EL$ surface, 3000 and 4200 for the $SQSBDE$ surface and 2800 and 3400 for the $SO–3$ PES. The exact sizes are given in table 3.3.

PES	Γ	$\vert 00\rangle$	$\{\vert 01\rangle, \vert 10\rangle\}$	$\{\vert 02\rangle, \vert 20\rangle\}$	$\vert 11\rangle$	E^{min}	E^{max}
$ES1$–EL	A_1	0.37	0.30	0.26	0.26	1800	3800
	B_1	0.02	0.02	0.02	0.02		
	A_2	0.34	0.28	0.32	0.26		
	B_2	0.32	0.41	0.26	0.26		
$SQSBDE$	A_1	0.24	0.38	0.34	0.34	2900	4900
	B_1	0.02	0.02	0.02	0.02		
	A_2	0.30	0.32	0.32	0.36		
	B_2	0.32	0.38	0.38	0.42		
SO–3	A_1	0.24	0.38	0.26	0.34	2900	4900
	B_1	0.02	0.02	0.02	0.02		
	A_2	0.18	0.25	0.20	0.25		
	B_2	0.24	0.38	0.30	0.26		

Table 3.2: Fractions of the dimensions of the primitive bases, and energy boundaries for the $\vert 00\rangle$ functions that are taken into the contracted basis. The energy boundaries E^{min} and E^{max} are in wavenumbers (cm^{-1}).

PES	A_1	B_1	A_2	B_2
$ES1$–EL	5977	3581	4047	4151
$SQSBDE$	4014	3083	3538	4153
SO–3	3439	2823	2793	3239

Table 3.3: Contracted basis sizes for the energy surfaces studied and all irreps.

Chapter 4

Results

In this chapter the results of the calculations on the ground state and first vibrationally excited state are given. The first section deals with the HCl dimer, whereas the HF dimer is discussed in section 4.2.

4.1 The HCl dimer

In table 4.1 the first ten eigenvalues of the Hamiltonian are shown for the ground state of $(HCl)_2$ on the $ES1$ PES, for all four irreps. In table 4.2 the same results are shown for the calculations on the $ES1{-}EL$ PES. The difference in energy between the calculations on the basis with free monomer stretch functions and the dimer adapted stretch functions was at most 0.02cm^{-1}. Therefore, only the results with the dimer adapted functions are shown.

i	A_1	B_1	A_2	B_2
1	0.00	187.33	164.65	14.97
2	53.63	242.49	216.02	79.31
3	72.38	274.31	234.66	103.88
4	112.05	291.21	264.28	137.49
5	133.47	326.04	287.59	165.34
6	148.31	334.68	307.42	188.31
7	165.87	364.64	319.30	190.36
8	187.04	367.11	332.12	218.61
9	207.94	376.17	345.76	235.90
10	214.63	398.45	367.14	245.88

Table 4.1: Eigenvalues of the $(HCl)_2$ ground state on the $ES1$ PES for $J = |K| = 0$. Values are given in wavenumbers (cm^{-1}), relative to the ground state energy of -417.04cm^{-1}.

In tables 4.3 and 4.4 the calculated eigenvalues for the vibrationally excited states on the $ES1$–EL surface are given. In these tables also the contributions of the vibrationally excited basis functions $\{|\,01\rangle, |\,10\rangle\}$ and the ground state function $|\,00\rangle$ are given, as well as the length of the residual vector.

i	A_1	B_1	A_2	B_2
1	0.00	189.98	166.98	15.23
2	54.09	245.69	218.81	80.16
3	73.37	277.79	237.87	105.28
4	113.11	295.00	267.67	138.99
5	135.15	330.03	291.39	167.36
6	150.42	339.08	311.44	190.88
7	167.61	368.84	323.13	192.70
8	189.38	371.61	336.48	221.21
9	210.66	380.99	350.41	238.82
10	217.08	403.64	371.85	249.21

Table 4.2: Eigenvalues of the $(HCl)_2$ ground state on the $ES1$–EL PES for $J = |K| = 0$. Values are given in wavenumbers (cm^{-1}), relative to the ground state energy of $-425.25cm^{-1}$.

	A_1				B_1			
i	E	$\|01\rangle$	$\|00\rangle$	r	E	$\|01\rangle$	$\|00\rangle$	r
1	2857.01	99.91	0.03	0.87	3031.50	99.94	0.01	1.21
2	2876.70	99.89	0.07	4.42	3054.08	99.94	0.02	1.27
3	2912.54	99.88	0.06	3.43	3084.52	99.95	0.01	1.31
4	2931.99	99.92	0.03	0.99	3103.08	99.94	0.01	1.26
5	2942.53	99.96	0.01	1.13	3110.87	99.95	0.02	1.38
6	2967.24	99.95	0.01	1.40	3134.60	99.96	0.01	1.41
7	2972.94	99.93	0.02	1.19	3141.69	99.94	0.02	1.45
8	2995.01	99.93	0.02	1.13	3157.09	99.95	0.01	1.47
9	3002.50	99.97	0.00	0.98	3161.73	99.95	0.01	1.44
10	3011.23	99.93	0.02	1.16	3179.46	99.96	0.01	1.45

Table 4.3: Eigenvalues of the first vibrationally excited $(HCl)_2$ state on the $ES1$–EL PES for $J = |K| = 0$ and A_1 and B_1 symmetry. Given are the energies in wavenumbers (cm^{-1}), the contribution of the excited and ground state monomer stretch basis functions to the resulting eigenvector in percent and the length of the residual vector in wavenumbers. The energies are relative to the ground state of $-425.25cm^{-1}$.

4.2 The HF dimer

In table 4.5 the results of the calculations on $(HF)_2$ on the $SQSBDE$ PES with dimer adapted monomer stretch functions are shown. In table 4.6 the results for the same calculation with free monomer functions are given.

In table 4.7 the energy levels for $(HF)_2$ are given, as calculated on the SO–3 PES. Since the difference between the free monomer and dimer adapted stretch basis is typically in the order of $10^{-4}cm^{-1}$ only the results on the dimer adapted basis are given.

In tables 4.8 and 4.9 the calculated eigenvalues for the vibrationally excited HF dimer on the $SQSBDE$ PES are shown, together with the contributions of

i	A_2 E	$\|01\rangle$	$\|00\rangle$	r	B_2 E	$\|01\rangle$	$\|00\rangle$	r
1	3029.62	99.92	0.03	1.53	2859.47	99.94	0.01	1.29
2	3055.72	99.94	0.01	1.17	2874.38	99.93	0.02	1.51
3	3082.76	99.94	0.02	1.81	2915.12	99.96	0.01	1.47
4	3101.55	99.94	0.02	1.62	2933.93	99.94	0.01	1.55
5	3112.28	99.95	0.01	1.27	2940.64	99.80	0.16	7.18
6	3133.03	99.94	0.02	2.19	2964.95	99.92	0.03	1.76
7	3143.23	99.95	0.01	1.28	2975.30	99.96	0.01	1.59
8	3156.00	99.94	0.02	1.92	2996.42	99.82	0.14	7.12
9	3162.73	99.95	0.01	1.31	3001.12	99.95	0.01	1.72
10	3178.09	99.95	0.02	2.22	3013.31	99.96	0.01	1.53

Table 4.4: Eigenvalues of the first vibrationally excited $(HCl)_2$ state on the $ES1$–EL PES for $J = |K| = 0$ and A_2 and B_2 symmetry. Given are the energies in wavenumbers (cm^{-1}), the contribution of the excited and ground state monomer stretch basis functions to the resulting eigenvector in percent and the length of the residual vector in wavenumbers. The energies are relative to the ground state of $-425.25cm^{-1}$.

i	A_1	B_1	A_2	B_2
1	0.00	380.57	378.83	0.44
2	126.40	493.97	491.29	127.37
3	160.62	574.81	544.68	168.08
4	244.58	598.94	594.54	246.23
5	275.03	679.82	641.55	289.14
6	292.74	696.34	688.74	339.22
7	355.37	773.80	690.09	357.49
8	385.03	784.61	732.00	402.61
9	400.05	790.52	779.18	440.37
10	425.37	846.28	788.57	455.62

Table 4.5: Eigenvalues of the $(HF)_2$ ground state on the $SQSBDE$ PES for $J = |K| = 0$. Values are given in wavenumbers (cm^{-1}), relative to the ground state energy of $-1057.88cm^{-1}$.

the ground and excited monomer stretch functions and the length of the residual vector. A state was considered to be (partially) excited when the contribution of the excited stretch functions was greater then 10%. The same holds for the results on the SO–3 PES, which are given in tables 4.10 and 4.11.

It can be seen that, especially for the $SQSBDE$ calculations, significant mixing of the ground and excited states occurs. This causes a shift in the energy levels, which results in a rapidly increasing uncertainty in the energy.

i	A_1	B_1	A_2	B_2
1	0.00	380.48	378.73	0.44
2	126.33	493.82	491.13	127.31
3	160.57	574.69	544.53	168.05
4	244.47	598.72	594.32	246.11
5	274.94	679.64	641.33	289.04
6	292.64	696.08	688.48	339.17
7	355.19	773.59	689.92	357.31
8	384.88	784.43	731.73	402.45
9	399.89	790.26	778.89	440.27
10	425.27	846.08	788.37	455.45

Table 4.6: Eigenvalues of the $(HF)_2$ ground state on the *SQSBDE* PES with monomer radial basis functions from free monomers for $J = |K| = 0$. Values are given in wavenumbers (cm^{-1}), relative to the ground state energy of $-1057.46cm^{-1}$.

i	A_1	B_1	A_2	B_2
1	0.00	423.09	420.86	0.59
2	126.57	546.36	542.87	129.69
3	162.92	605.06	571.47	170.11
4	248.21	659.00	654.77	254.51
5	273.03	724.00	685.22	299.55
6	306.12	760.95	716.10	341.50
7	367.54	814.28	755.35	373.04
8	392.08	832.29	788.15	421.29
9	425.18	857.22	831.30	468.57
10	446.55	911.16	848.85	482.03

Table 4.7: Eigenvalues of the $(HF)_2$ ground state on the *SO*–3 PES for $J = |K| = 0$. Values are given in wavenumbers (cm^{-1}), relative to the ground state energy of $-1061.71cm^{-1}$.

	A_1				B_1			
i	E	$\|01\rangle$	$\|00\rangle$	r	E	$\|01\rangle$	$\|00\rangle$	r
1	3895.94	92.25	7.69	64.97	4283.74	99.08	0.85	23.90
2	3939.94	99.91	0.04	3.87	4312.42	99.89	0.05	4.78
3	4034.47	99.89	0.06	6.25	4405.39	99.67	0.26	13.40
4	4064.44	99.88	0.06	5.10	4424.16	99.90	0.03	2.04
5	4065.58	99.82	0.13	8.40	4464.58	99.86	0.08	7.25
6	4100.75	99.92	0.03	3.06	4490.18	99.92	0.03	3.50
7	4161.09	92.91	7.03	66.42	4515.92	97.84	2.08	38.37
8	4181.74	99.89	0.03	3.83	4527.68	99.86	0.04	3.99
9	4190.27	97.47	2.47	40.48	4566.03	83.68	16.27	110.53
10	4206.48	96.29	3.66	41.92	4566.21	16.22	83.77	251.78

Table 4.8: Eigenvalues of the first vibrationally excited $(HF)_2$ state on the *SQSBDE* PES for $J = |K| = 0$ and A_1 and B_1 symmetry. Given are the energies in wavenumbers (cm^{-1}), the contribution of the excited and ground state monomer stretch basis functions to the resulting eigenvector in percent and the length of the residual vector in wavenumbers. The energies are relative to the ground state of $-1057.88cm^{-1}$.

	A_2				B_2			
i	E	$\|01\rangle$	$\|00\rangle$	r	E	$\|01\rangle$	$\|00\rangle$	r
1	4283.33	98.74	1.18	26.37	3896.04	99.90	0.05	4.09
2	4312.92	99.90	0.03	3.13	3939.82	99.93	0.02	2.01
3	4404.46	23.26	76.72	230.60	4034.89	96.56	3.38	46.96
4	4404.63	76.55	23.39	127.43	4063.63	21.41	78.57	222.37
5	4425.12	96.87	3.06	47.63	4063.68	78.50	21.45	116.22
6	4459.39	99.84	0.10	7.30	4067.57	99.83	0.11	8.04
7	4496.67	41.63	58.34	195.40	4098.45	18.22	81.77	243.16
8	4496.69	58.26	41.70	165.32	4098.49	81.71	18.25	114.50
9	4514.26	97.93	1.98	38.73	4162.32	99.14	0.79	23.42
10	4529.58	99.77	0.14	9.27	4180.19	99.77	0.15	9.12

Table 4.9: Eigenvalues of the first vibrationally excited $(HF)_2$ state on the *SQSBDE* PES for $J = |K| = 0$ and A_2 and B_2 symmetry. Given are the energies in wavenumbers (cm^{-1}), the contribution of the excited and ground state monomer stretch basis functions to the resulting eigenvector in percent and the length of the residual vector in wavenumbers. The energies are relative to the ground state of $-1057.88cm^{-1}$.

	A_1				B_1			
i	E	$\|01\rangle$	$\|00\rangle$	r	E	$\|01\rangle$	$\|00\rangle$	r
1	3867.10	99.59	0.33	10.51	4303.58	95.88	4.03	45.49
2	3929.18	99.50	0.39	11.91	4353.25	98.83	1.05	22.35
3	4000.50	99.79	0.13	7.02	4432.99	97.97	1.93	32.37
4	4043.22	99.72	0.21	9.23	4475.17	99.83	0.06	4.72
5	4056.93	98.44	1.45	21.75	4480.79	99.31	0.60	18.26
6	4096.21	99.85	0.05	3.83	4514.15	99.85	0.06	4.94
7	4128.44	96.12	3.79	38.63	4552.37	98.95	0.94	20.77
8	4161.48	98.49	1.44	25.09	4590.39	99.82	0.04	3.43
9	4182.62	96.90	2.99	35.82	4599.97	99.52	0.40	13.37
10	4196.84	99.07	0.85	18.86	4629.32	99.85	0.07	5.91

Table 4.10: Eigenvalues of the first vibrationally excited $(HF)_2$ state on the $SO{-}3$ PES for $J = |K| = 0$ and A_1 and B_1 symmetry. Given are the energies in wavenumbers (cm^{-1}), the contribution of the excited and ground state monomer stretch basis functions to the resulting eigenvector in percent and the length of the residual vector in wavenumbers. The energies are relative to the ground state of $-1061.71 cm^{-1}$.

	A_2				B_2			
i	E	$\|01\rangle$	$\|00\rangle$	r	E	$\|01\rangle$	$\|00\rangle$	r
1	4303.05	99.53	0.38	12.72	3867.27	97.98	1.94	28.38
2	4353.89	98.23	1.65	24.68	3929.00	99.81	0.08	5.62
3	4431.98	99.75	0.15	7.74	4001.39	99.27	0.64	14.11
4	4469.78	99.64	0.27	10.56	4045.43	99.35	0.58	16.16
5	4479.09	99.76	0.12	6.75	4055.55	99.82	0.07	5.13
6	4523.56	99.25	0.66	19.49	4094.14	99.86	0.04	3.45
7	4551.17	99.40	0.49	14.72	4130.62	98.81	1.10	22.61
8	4588.57	96.09	3.80	42.71	4168.44	95.69	4.24	40.81
9	4594.29	99.56	0.31	11.69	4181.23	99.59	0.32	12.98
10	4618.01	99.74	0.17	9.49	4200.10	99.40	0.52	14.70

Table 4.11: Eigenvalues of the first vibrationally excited $(HF)_2$ state on the $SO{-}3$ PES for $J = |K| = 0$ and A_2 and B_2 symmetry. Given are the energies in wavenumbers (cm^{-1}), the contribution of the excited and ground state monomer stretch basis functions to the resulting eigenvector in percent and the length of the residual vector in wavenumbers. The energies are relative to the ground state of $-1061.71 cm^{-1}$.

Chapter 5

Discussion and conclusion

5.1 Ground state HX dimer

In table 5.1 an overview is given for some of the characteristics of the HCl dimer. The indices $(\nu_3\nu_4\nu_5\nu_6)$ in the table denote the intermolecular modes of the dimer, and indicate the *cis*-bending, intermolecular stretch, *trans*-bending and torsional motions of the dimer respectively. The assignments of the state labels are taken from [6]. As can be seen in table 5.1 the dissociation energy from the present

	$ES1$	Ref.[5]	$ES1{-}EL$	Ref.[6]	Exp.
D_0	−417.04	−416.25	−425.25	−425.26	−431
(0010) − (0000)	14.97	14.95	15.23	15.26	15.47668
(0020) − (0010)	38.66	38.54	38.86	38.69	37.64540
(0001) − (0000)	164.65	164.21	166.98	166.99	160.778
(0011) − (0000)	187.33	186.79	189.98	190.01	184.862

Table 5.1: Overview of some characteristics of the HCl dimer from present calculations, 6D calculations from literature, and experimental results. All values are in wavenumbers (cm^{-1}). Experimental data are taken from Refs. [7], [9] and [15].

calculation on the $ES1$ PES is slightly bigger then that reported by Qiu and Bačić [5]. The ν_5 ground state tunneling splitting is virtually the same, but bigger differences occur for the (0020), (0001) and (0011) levels. The results on the $ES1$–EL PES are closer to the results of Qiu, Zhang and Bačić [6]. The ground state tunneling splitting and ν_6 splittings are virtually the same, as is the dissociation energy. Only the ν_5 overtone splitting shows a somewhat bigger difference. A possible explanation of why the $ES1$ results differ more from literature then the $ES1{-}EL$ results may be that in this report all calculations were done using a monomer vibrational basis consisting of six functions ($v_A + v_B \leq 2$), whereas Qiu and Bačić used only two functions per monomer in their $ES1$ calculations. This supposition is supported by the fact that the variational calculations in this report lead to lower lying energy levels, indicating a better convergence of these levels.

The $(HF)_2$ ground state was also calculated on two different potential surfaces.

Some results are shown in table 5.2, together with results of the calculations by Zhang *et al.* on the *SQSBDE* PES and experimental numbers. Unfortunately, no results of calculations on the $SO\!-\!3$ surface were found in literature, so no comparison could be made for this potential. The states are labeled in the same way as the $(HCl)_2$ states, with the assignments taken from [3]. The first column of

	SQSBDE *free*	*SQSBDE* *adapt.*	Ref.[3]	SO–3	Exp.
D_0	−1057.46	−1057.88	−1057.33	−1061.71	−1062
(0010) − (0000)	0.44	0.44	0.44	0.59	0.65869
(0020) − (0010)	160.13	160.18	160.14	162.33	
(0001) − (0000)	378.73	378.83	378.72	420.86	
(0011) − (0000)	380.48	380.57	380.47	423.09	

Table 5.2: Overview of some characteristics of the HF dimer from present calculations, 6D calculations from literature, and experimental results. The first column shows the results from calculations with free monomer stretch functions on the *SQSBDE* PES, the second with dimer adapted functions. All values are in wavenumbers (cm^{-1}). Experimental data are taken from Refs. [10] and [11].

table 5.2 shows the results on the *SQSBDE* surface with the free monomer stretch basis. Although the dissociation energy is somewhat higher then that calculated by Zhang *et al.*, the splittings shown are virtually the same. The difference in dissociation energy is caused by the fact that for the calculations in this report more monomer stretch basis functions were used then in the calculations by Zhang *et al.*. This was confirmed by doing the calculations in the smaller basis. Using dimer adapted stretch functions results in a dissociation energy that is yet another $0.4\mathrm{cm}^{-1}$ higher. The ground state tunneling splitting remains the same, but the ν_6 fundamental splittings increase by $0.1\mathrm{cm}^{-1}$.

Since there are no 6D results on the $SO\!-\!3$ PES available in literature, it can only be checked against experimental data. Comparison of the splittings from table 5.2 does show that it reproduces the experimental data better. The dissociation energy of $1061.71\mathrm{cm}^{-1}$ compares very well with the experimental value of $1062 \pm 1\mathrm{cm}^{-1}$ [10]. The value for the ground state tunneling splitting is about 90% of the experimental value, compared to 67% with the *SQSBDE* potential.

5.2 Vibrationally excited HX dimer

In table 5.3 an overview of some characteristics of the vibrationally excited $(HCl)_2$ are shown. The states are labeled by $(\nu_1\nu_2\nu_3\nu_4\nu_5\nu_6)$, where ν_1 indicates the "free" monomer stretching vibration, ν_2 the "bound" monomer stretch, and ν_3 up to ν_6 are the intermolecular modes from section 5.1. The assignments of the labels to the energy levels are taken from [6]. The wave functions of the excited HCl dimer are not so heavily mixed, and hence quite well converged. The maximum error bound is $7.18\mathrm{cm}^{-1}$ for the fifth B_2 state, but generally the error bounds are $\sim 1\mathrm{cm}^{-1}$, which in practice means that the eigenvalues are converged up to at least $0.01\mathrm{cm}^{-1}$. The splitting given in table 5.3 are in perfect agreement with

	$ES1$–EL	Ref. [6]	Exp.
(010000) – (000000)	2857.01	2856.98	2854.059
(100000) – (000000)	2876.70	2876.69	2880.250
(010010) – (010000)	2.46	2.45	3.176
(100010) – (100000)	−2.32	−2.31	−3.324
(010020) – (010010)	53.07	52.92	
(100020) – (100010)	92.86	92.84	
(010001) – (010000)	172.61	172.63	
(100001) – (100000)	179.02	179.03	
(010011) – (010010)	172.03	172.05	
(100011) – (100010)	179.70	179.70	

Table 5.3: Overview of some characteristics of HCl stretching excited $(HCl)_2$ from present calculations, 6D calculations from literature and experiment. All values are in wavenumbers (cm^{-1}). Experimental data are taken from Ref. [8].

those by Qiu, Zhang and Bačić [6]. Only the ν_5 overtone in the ν_2 fundamental shows a deviation that exceeds $0.02 cm^{-1}$.

The results on the vibrationally excited HF dimer calculations are less accurate then the HCl dimer results. As can be seen in tables 4.8 up to 4.11 heavy mixing occurs between high-lying vibrational ground state functions and the lower vibrationally excited states. This effect causes shifts in the resulting energy levels of the mixed functions, which leads to higher uncertainties, up to $\sim 200 cm^{-1}$, in this energy. Although the energies are usually far better converged then may be expected from the error bound, the shift must still be considerable.

The mixing occurs because high-lying vibrational ground states are shifted a great deal when reducing the basis. This is due to the fact that in doing so only the effect of coupling between $(\nu_1\nu_2) = (00)$ and $\{(01),(10)\}$ functions on the vibrationally excited state was taken into account. Hence, only the functions that have an effect on the excited states are in the basis, thereby neglecting the effect that the reduction has on the vibrational ground states. Important matrix elements that couple the ground state functions with the excited functions are thereby lost, which causes the large shift in the ground state energies. The shifting of the vibrational ground state levels around the vibrational excitation energy may cause one of these levels to become almost degenerate with a vibrationally excited level, thereby perturbing it. This can be seen in tables 4.8 and 4.9, where the mixing of some levels is so heavy that both mixing levels are included in the table for certain states. One can see that the energy difference between the heavily mixed levels is very small when compared to the splitting with the nearest excited state in the same symmetry block (by more then a factor 100).

Although the excited states may not be so well converged, we can still make some comparison with other 6D calculations and experimental data. In table

5.4 an overview is given for some characteristic splittings in vibrationally excited $(HF)_2$. The labeling of the states is the same as for the excited HCl dimer. The assignments of the labels to the $SQSBDE$ states was taken from [4]. The same order of labels was used in assigning the SO–3 levels, with the exception of the (010020) and the (100100) levels. These levels were switched, since experimentally (Ref. [14]) it is shown that the (010020) level is lower in energy then the (100100) state, whereas the assignment by Zhang and Zhang for the $SQSBDE$ PES shows the opposite.

	$SQSBDE$	Ref.[4]	SO–3	Exp.
(010000) – (000000)	3895.94	3896.39	3867.10	3868.079
(100000) – (000000)	3939.94	3940.64	3929.18	3930.903
(010010) – (010000)	0.08	0.09	0.17	0.234
(100010) – (100000)	−0.12	−0.13	−0.18	−0.215
(010020) – (010010)	169.54	169.48	175.95	178.433
(100020) – (100010)	160.93	160.79	167.21	166.738
(010100) – (010000)	138.53	138.48	133.40	132.616
(100100) – (100000)	124.50	124.23	127.75	127.573

Table 5.4: Overview of some characteristics of HF stretching excited $(HF)_2$ from present calculations, 6D calculations from literature and experiment. All values are in wavenumbers (cm^{-1}). Experimental data are taken from Refs. [12] and [13].

Comparison of the calculated splittings with those by Wu, Zhang and Zhang [4] shows that the differences are not very large. The position of the ν_1 and ν_2 fundamentals are in reasonable accordance with literature, and the ν_5 tunneling splittings are virtually the same. There are small deviations in the ν_5 overtone and the ν_4 fundamental. No calculations on the SO–3 PES have so far been reported in literature, which is why we can only compare with experimental results. Inspection of table 5.4 does show that all splittings from this surface are in far better agreement with experiment then those produced by the $SQSBDE$ potential. The ν_1 and ν_2 tunneling splittings of 0.17 and -0.18cm^{-1} represent 73% and 84% of the experimental values, whereas the $SQSBDE$ PES only reproduces 38% and 60%. Other deviations lie in the range $0.2-2.5\text{cm}^{-1}$, compared to $3-9\text{cm}^{-1}$ on the $SQSBDE$ surface. Since the SO–3 surface also reproduces the ground state far better, we can safely conclude that using this PES results in a better description of the HF dimer then using the $SQSBDE$ potential.

5.3 Conclusion and outlook

Ground state calculations on the HCl and HF dimers were reported, and the results are in good agreement with full dimensional calculations from literature. Also calculations on HX stretching excited HX dimers were performed, leading to results that are in perfect (X = Cl) or good (X = F) agreement with other calculations. Part of the deviations in the excited $(HF)_2$ calculations may be due to neglect of the effect of coupling between ground state and excited monomer stretch functions on the vibrational ground state levels in the region of the vibrational excitation energy. This causes a shift of these levels, which leads to mixing with some of the excited levels studied, thereby perturbing them. New calculations need to be done, where this effect is taken into account. Also the near absence of this effect in the HCl dimer should be studied. The study does show that the SO–3 potential performs a lot better then the $SQSBDE$ potential. All calculations in this report were done with $J = 0$. Future calculations can be done for other J, which also may have to take the Coriolis coupling not present for $J = 0$ into account.

Bibliography

[1] A. van der Avoird, P.E.S Wormer, R. Moszynski, *Chem. Rev.*, **1994**, *94*, 1931

[2] G.C. Groenenboom, D.T. Colbert, *J. Chem. Phys.*, **1993**, *99*, 9681

[3] D.H. Zhang, Q. Wu, J.Z.H. Zhang, M. von Dirke, Z. Bačić, *J. Chem. Phys.*, **1994**, *102*, 2315

[4] Q. Wu, D.H. Zhang, J.Z.H. Zhang, *J. Chem. Phys.*, **1995**, *103*, 2548

[5] Y. Qiu, Z. Bačić, *J. Chem. Phys.*, **1997**, *106*, 2158

[6] Y. Qiu, J.Z.H. Zhang, Z. Bačić, *J. Chem. Phys.*, **1998**, *108*, 4804

[7] G.A. Blake, R.E. Bumgarner, *J. Chem. Phys.*, **1989**, *91*, 7300

[8] M.D. Schuder, C.M. Lovejoy, R. Lascola, D.J. Nesbitt, *J. Chem. Phys.*, **1993**, *99*, 4346

[9] A.S. Pine, B.J. Howard, *J. Chem. Phys.*, **1986**, *84*, 590

[10] E.J. Bohac, M.D. Marshall, R.E. Miller, *J. Chem. Phys.*, **1992**, *96*, 6681

[11] W.J. Lafferty, R.D. Suenram, F.J. Lovas, *J. Mol. Spec.*, **1987**, *123*, 434

[12] K. von Puttkamer, M. Quack, *Chem. Phys.*, **1989**, *139*, 31

[13] D.T. Anderson, S. Davis, D.J. Nesbitt, *J. Chem. Phys.*, **1996**, *105*, 4488

[14] D.T. Anderson, S. Davis, D.J. Nesbitt, *J. Chem. Phys.*, **1996**, *104*, 6225

[15] M.J. Elrod, R.J. Saykally, *J. Chem. Phys.*, **1995**, *103*, 933

[16] M. Quack, M.A. Suhm, *J. Chem. Phys.*, **1991**, *95*, 28

[17] W. Klopper, M. Quack, M.A. Suhm, *J. Chem. Phys.*, **1998**, *108*, 10096

[18] P.R. Bunker, P. Jensen, *Molecular Symmetry And Spectroscopy*, NRC Research Press: Ottawa, **1998**

Appendix A

Angular momentum

A general angular momentum operator $\hat{\boldsymbol{\lambda}}$ operating on the space fixed angles $(\phi^{SF}, \theta^{SF}, \psi^{SF})$ has components

$$\hat{\boldsymbol{\lambda}}^{SF} = \begin{pmatrix} \hat{\lambda}_x^{SF} \\ \hat{\lambda}_y^{SF} \\ \hat{\lambda}_z^{SF} \end{pmatrix} = i\hbar \begin{pmatrix} \cos\phi \cot\theta \frac{\partial}{\partial\phi} + \sin\phi \frac{\partial}{\partial\theta} - \frac{\cos\phi}{\sin\theta}\frac{\partial}{\partial\psi} \\ \sin\phi \; cot\theta \frac{\partial}{\partial\phi} - \cos\phi \frac{\partial}{\partial\theta} - \frac{\sin\phi}{\sin\theta}\frac{\partial}{\partial\psi} \\ -\frac{\partial}{\partial\phi} \end{pmatrix} . \tag{A.1}$$

This operator satisfies the usual commutation relations for angular momentum operators, i.e.

$$\left[\hat{\lambda}_i^{SF}, \hat{\lambda}_j^{SF}\right] = i\hbar \sum_k \epsilon_{ijk} \hat{\lambda}_k^{SF} \quad , \tag{A.2}$$

where ϵ_{ijk} is the Levi-Civita anti-symmetric tensor

$$\epsilon_{ijk} = \begin{cases} 0 & \text{if two or more indices are equal} \\ 1 & \text{if } ijk \text{ is an even permutation of 123} \\ -1 & \text{if } ijk \text{ is an odd permutation of 123} \end{cases} . \tag{A.3}$$

When changing to BF coordinates we get $\hat{\boldsymbol{\lambda}}^{BF} = \mathbb{R}(\phi^{SF}, \theta^{SF}, \psi^{SF})^T \hat{\boldsymbol{\lambda}}^{SF}$ operating on the body fixed Euler angles $(\phi^{BF}, \theta^{BF}, \psi^{BF})$, where the rotation matrix $\mathbb{R}(\phi^{SF}, \theta^{SF}, \psi^{SF}) = \mathbb{R}_z(\phi^{SF})\mathbb{R}_y(\theta^{SF})\mathbb{R}_z(\psi^{SF})$ is defined by

$$\mathbb{R}_z(\vartheta) = \begin{pmatrix} \cos\vartheta & -\sin\vartheta & 0 \\ \sin\vartheta & \cos\vartheta & 0 \\ 0 & 0 & 1 \end{pmatrix}, \quad \mathbb{R}_y(\vartheta) = \begin{pmatrix} \cos\vartheta & 0 & \sin\vartheta \\ 0 & 1 & 0 \\ -\sin\vartheta & 0 & \cos\vartheta \end{pmatrix}. \tag{A.4}$$

Performing the required matrix multiplication leads us to

$$\hat{\boldsymbol{\lambda}}^{BF} = \begin{pmatrix} \hat{\lambda}_x^{BF} \\ \hat{\lambda}_y^{BF} \\ \hat{\lambda}_z^{BF} \end{pmatrix} = i\hbar \begin{pmatrix} \frac{\cos\psi}{\sin\theta}\frac{\partial}{\partial\phi} - \sin\psi \frac{\partial}{\partial\theta} - \cos\psi \cot\theta \frac{\partial}{\partial\psi} \\ -\frac{\sin\psi}{\sin\theta}\frac{\partial}{\partial\phi} - \cos\psi \frac{\partial}{\partial\theta} + \sin\psi \cot\theta \frac{\partial}{\partial\psi} \\ -\frac{\partial}{\partial\psi} \end{pmatrix} . \tag{A.5}$$

The body fixed operator does not satisfy the usual commutation relations of Eq. (A.2), but rather the so-called "anomalous" ones

$$\left[\hat{\lambda}_i^{BF}, \hat{\lambda}_j^{BF}\right] = -i\hbar \sum_k \epsilon_{ijk} \hat{\lambda}_k^{BF} \quad . \tag{A.6}$$

In [1] it is shown that the dimer end-over-end angular momentum operator $\hat{\mathbf{l}}^{SF} = \hat{\lambda}^{SF}(\alpha, \beta, 0)$ can be written as

$$(\hat{l}^{SF})^2 = (\hat{J}^{SF})^2 + (\hat{\mathbf{j}}_A + \hat{\mathbf{j}}_B)^2 - 2(\hat{\mathbf{j}}_A + \hat{\mathbf{j}}_B) \cdot \hat{\mathbf{J}}, \tag{A.7}$$

where

$$\hat{\mathbf{J}} = \begin{pmatrix} \hat{J}_x \\ \hat{J}_y \\ \hat{J}_z \end{pmatrix} = i\hbar \begin{pmatrix} \frac{1}{\sin\beta}\frac{\partial}{\partial\alpha} + \cot\beta(\frac{\partial}{\partial\phi_A^{BF}} + \frac{\partial}{\partial\phi_B^{BF}}) \\ -\frac{\partial}{\partial\beta} \\ -(\frac{\partial}{\partial\phi_A^{BF}} + \frac{\partial}{\partial\phi_B^{BF}}) \end{pmatrix} \tag{A.8}$$

and

$$\hat{\mathbf{J}}^{SF} = \mathbb{R}(\alpha, \beta, 0)\hat{\mathbf{J}} \quad = \quad \hat{\boldsymbol{\lambda}}^{SF}(\alpha, \beta, \frac{\phi_A^{BF} + \phi_B^{BF}}{2}) \tag{A.9}$$

$$\hat{\mathbf{j}}_X \quad = \quad \hat{\boldsymbol{\lambda}}^{SF}(\phi_X^{BF}, \theta_X^{BF}, \psi_X^{BF}) \tag{A.10}$$

Note that $\hat{\mathbf{J}}$ does not satisfy the normal angular momentum commutation relations, nor the anomalous ones, which is why it is often referred to as a pseudo-angular momentum operator.

For linear molecules, as the monomers in $(HX)_2$ are, there exists no dependence on ψ. The angular momentum operators for such molecules can thus be obtained from Eqs. (A.1) and (A.5) by omitting the $\frac{\partial}{\partial\psi}$ terms, and setting ψ to 0.

Appendix B

Transformation of coordinates

In this section the effects of the symmetry operations $\hat{E}^*$ and $\hat{P}$ on the coordinates of the dimer are derived. In a space fixed frame we write the positions of the atoms X_A, H_A, X_B and H_B as $\mathbf{r}_1$, $\mathbf{r}_2$, $\mathbf{r}_3$ and $\mathbf{r}_4$ respectively (see figure 2.1). The vectors $\mathbf{r}_A^{SF}$, $\mathbf{r}_B^{SF}$ and $\mathbf{R}$ are then defined by

$$\mathbf{r}_A^{SF} = \mathbf{r}_2 - \mathbf{r}_1 \tag{B.1}$$

$$\mathbf{r}_B^{SF} = \mathbf{r}_4 - \mathbf{r}_3 \tag{B.2}$$

$$\mathbf{R} = \frac{1}{m_B}(m_3\mathbf{r}_3 + m_4\mathbf{r}_4) - \frac{1}{m_A}(m_1\mathbf{r}_1 + m_2\mathbf{r}_2), \tag{B.3}$$

where m_A and m_B are the total masses of diatoms A and B. Since for HX dimers $m_1 = m_3 = m_{\mathrm{X}}$, $m_2 = m_4 = m_{\mathrm{H}}$ and $m_A = m_B = m_{\mathrm{HX}}$ the expression for $\mathbf{R}$ becomes

$$\mathbf{R} = \frac{1}{m_{\mathrm{HX}}}\left[m_{\mathrm{X}}(\mathbf{r}_3 - \mathbf{r}_1) + m_{\mathrm{H}}(\mathbf{r}_4 - \mathbf{r}_2)\right]. \tag{B.4}$$

$\hat{E}^*$ and $\hat{P}$ are defined by

$$\hat{E}^* : \left\{ \begin{array}{lcl} \mathbf{r}_1 & \to & -\mathbf{r}_1 \\ \mathbf{r}_2 & \to & -\mathbf{r}_2 \\ \mathbf{r}_3 & \to & -\mathbf{r}_3 \\ \mathbf{r}_4 & \to & -\mathbf{r}_4 \end{array} \right. \qquad \hat{P} : \left\{ \begin{array}{lcl} \mathbf{r}_1 & \to & \mathbf{r}_3 \\ \mathbf{r}_2 & \to & \mathbf{r}_4 \\ \mathbf{r}_3 & \to & \mathbf{r}_1 \\ \mathbf{r}_4 & \to & \mathbf{r}_2 \end{array} \right. . \tag{B.5}$$

Combining Eqs. (B.1), (B.2), (B.4) and (B.5) we see that

$$\hat{E}^* : \left\{ \begin{array}{rcl} \mathbf{r}_A^{SF} & \to & -\mathbf{r}_A^{SF} \\ \mathbf{r}_B^{SF} & \to & -\mathbf{r}_B^{SF} \\ \mathbf{R} & \to & -\mathbf{R} \end{array} \right. \qquad \hat{P} : \left\{ \begin{array}{rcl} \mathbf{r}_A^{SF} & \to & \mathbf{r}_B^{SF} \\ \mathbf{r}_B^{SF} & \to & \mathbf{r}_A^{SF} \\ \mathbf{R} & \to & -\mathbf{R} \end{array} \right. . \tag{B.6}$$

It is then easily verified that the space fixed polar coordinates of $\mathbf{R}$, $\mathbf{r}_A^{SF}$ and $\mathbf{r}_B^{SF}$ tranform as

$$\hat{E}^*:\left\{\begin{array}{ccc}\beta & \to & \pi-\beta\\ \alpha & \to & \pi+\alpha\\ R & \to & R\\ \theta_X^{SF} & \to & \pi-\theta_X^{SF}\\ \phi_X^{SF} & \to & \pi+\phi_X^{SF}\\ r_X & \to & r_X\end{array}\right. \qquad \hat{P}:\left\{\begin{array}{ccc}\beta & \to & \pi-\beta\\ \alpha & \to & \pi+\alpha\\ R & \to & R\\ \theta_X^{SF} & \to & \theta_Y^{SF}\\ \phi_X^{SF} & \to & \phi_Y^{SF}\\ r_X & \to & r_Y\end{array}\right. , \tag{B.7}$$

where $X, Y = A, B$ and $X \neq Y$.

The space fixed vectors $\mathbf{r}_A^{SF}$ and $\mathbf{r}_B^{SF}$ are connected to their body fixed counterparts by

$$\mathbf{r}_X^{SF} = \mathbb{R}_z(\alpha)\mathbb{R}_y(\beta)\mathbf{r}_X^{BF}, \tag{B.8}$$

where $\mathbb{R}_z$ and $\mathbb{R}_y$ are defined in Eq. (A.4). To determine the effect of the symmetry operations on the body fixed vectors we thus need to determine the effect on the rotation $\mathbb{R}_z(\alpha)\mathbb{R}_y(\beta)$. The effect on the angles α and β are given in Eq. (B.7), so by introducing the rotation matrix $\mathbb{R}_x$

$$\mathbb{R}_x(\vartheta) = \begin{pmatrix} 1 & 0 & 0\\ 0 & \cos\vartheta & -\sin\vartheta\\ 0 & \sin\vartheta & \cos\vartheta \end{pmatrix} \tag{B.9}$$

and using the relationships

$$\begin{aligned}\mathbb{R}_\alpha(\vartheta+\vartheta') &= \mathbb{R}_\alpha(\vartheta)\mathbb{R}_\alpha(\vartheta') \quad \alpha = x, y, z && \text{(B.10)}\\ \mathbb{R}_z(\pi)\mathbb{R}_y(\pi) &= \mathbb{R}_x(\pi) && \text{(B.11)}\\ \mathbb{R}_x(\pi)\mathbb{R}_y(-\vartheta) &= \mathbb{R}_y(\vartheta)\mathbb{R}_x(\pi) && \text{(B.12)}\end{aligned}$$

we can derive

$$\begin{aligned}\mathbb{R}_z(\pi+\alpha)\mathbb{R}_y(\pi-\beta) &= \mathbb{R}_z(\alpha)\mathbb{R}_z(\pi)\mathbb{R}_y(\pi)\mathbb{R}_y(-\beta)\\ &= \mathbb{R}_z(\alpha)\mathbb{R}_x(\pi)\mathbb{R}_y(-\beta)\\ &= \mathbb{R}_z(\alpha)\mathbb{R}_y(\beta)\mathbb{R}_x(\pi). && \text{(B.13)}\end{aligned}$$

Hence we write

$$\begin{aligned}\hat{E}^* &: \mathbf{r}_X^{SF} = \mathbb{R}_z(\alpha)\mathbb{R}_y(\beta)\mathbf{r}_X^{BF} \to -\mathbf{r}_X^{SF} = \mathbb{R}_z(\alpha)\mathbb{R}_y(\beta)\mathbb{R}_x(\pi)\mathbf{r'}_X^{BF} && \text{(B.14)}\\ \hat{P} &: \mathbf{r}_X^{SF} = \mathbb{R}_z(\alpha)\mathbb{R}_y(\beta)\mathbf{r}_X^{BF} \to \mathbf{r}_Y^{SF} = \mathbb{R}_z(\alpha)\mathbb{R}_y(\beta)\mathbb{R}_x(\pi)\mathbf{r'}_X^{BF} && \text{(B.15)}\end{aligned}$$

Solving for the $\mathbf{r'}_X^{BF}$, using the fact that $\mathbb{R}_x(\pi)^T = \mathbb{R}_x(\pi)$ gives

$$\begin{aligned}\hat{E}^* &: \mathbf{r}_X^{BF} \to -\mathbb{R}_x(\pi)\mathbf{r}_X^{BF} && \text{(B.16)}\\ \hat{P} &: \mathbf{r}_X^{BF} \to \mathbb{R}_x(\pi)\mathbf{r}_Y^{BF} && \text{(B.17)}\end{aligned}$$

Performing the required matrix multiplications and rewriting the resulting vectors in polar coordinates then gives

$$\hat{E}^*:\left\{\begin{array}{ccc}\beta & \to & \pi-\beta\\ \alpha & \to & \pi+\alpha\\ R & \to & R\\ \theta_X^{BF} & \to & \theta_X^{BF}\\ \phi_X^{BF} & \to & \pi-\phi_X^{BF}\\ r_X & \to & r_X\end{array}\right. \qquad \hat{P}:\left\{\begin{array}{ccc}\beta & \to & \pi-\beta\\ \alpha & \to & \pi+\alpha\\ R & \to & R\\ \theta_X^{BF} & \to & \pi-\theta_Y^{BF}\\ \phi_X^{BF} & \to & -\phi_Y^{BF}\\ r_X & \to & r_Y\end{array}\right. . \tag{B.18}$$

Finally, the effect of $\hat{P}^* = \hat{E}^*\hat{P} = \hat{P}\hat{E}^*$ is easily determined to be

$$\hat{P}^* : \left\{ \begin{array}{rcl} \beta & \rightarrow & \beta \\ \alpha & \rightarrow & \alpha \\ R & \rightarrow & R \\ \theta_X^{BF} & \rightarrow & \pi - \theta_Y^{BF} \\ \phi_X^{BF} & \rightarrow & \pi + \phi_Y^{BF} \\ r_X & \rightarrow & r_Y \end{array} \right. \tag{B.19}$$

Appendix C

Transformation of basis

In this appendix we will derive the effects of the operators $\hat{E}^*$ and $\hat{P}$ on the angular and vibrational basis functions. The effects of $\hat{E}^*$ and $\hat{P}$ on the coordinates of the dimer are given in Eq. (B.18. In this appendix we drop the BF label on the θ and ϕ angles.

Using the properties of the Racah normalized spherical harmonics and the Wigner D-matrices given in table C.1, the effect of $\hat{E}^*$ on the angular basis functions can be derived:

$$
\begin{aligned}
& \hat{E}^* | j_A, j_B, j, K; J, M\rangle \\
= \; & \hat{E}^* \left[D^{(J)}_{MK}(\alpha,\beta,0)^* \sum_{m_A,m_B} \langle jK | j_A m_A; j_B m_B \rangle C^{j_A}_{m_A}(\theta_A,\phi_A) C^{j_B}_{m_B}(\theta_B,\phi_B) \right] \\
= \; & D^{(J)}_{MK}(\pi+\alpha,\pi-\beta,0)^* \times \\
& \sum_{m_A,m_B} \langle jK | j_A m_A; j_B m_B \rangle C^{j_A}_{m_A}(\theta_A,\pi-\phi_A) C^{j_B}_{m_B}(\theta_B,\pi-\phi_B) \\
= \; & e^{iM\pi}(-1)^{J+M} D^{(J)}_{MK}(\alpha,\beta,0)^* \times \\
& \sum_{m_A,m_B} \langle jK | j_A m_A; j_B m_B \rangle C^{j_A}_{-m_A}(\theta_A,\phi_A) C^{j_B}_{-m_B}(\theta_B,\phi_B) \\
= \; & (-1)^J D^{(J)}_{MK}(\alpha,\beta,0)^* \times \\
& \sum_{m_A,m_B} \langle jK | j_A, -m_A; j_B, -m_B \rangle C^{j_A}_{m_A}(\theta_A,\phi_A) C^{j_B}_{m_B}(\theta_B,\phi_B)
\end{aligned}
$$

$C^l_m(\pi-\theta,\pi+\phi)$	$=$	$(-1)^l C^l_m(\theta,\phi)$
$C^l_m(\theta,\pi-\phi)$	$=$	$C^l_{-m}(\theta,\phi)$
$D^{(l)}_{mk}(\alpha+\omega,\beta,\gamma)$	$=$	$e^{-im\omega} D^{(l)}_{mk}(\alpha,\beta,\gamma)$
$D^{(l)}_{mk}(\alpha,\pi-\beta,-\gamma)$	$=$	$(-1)^{l+m} D^{(l)}_{mk}(\alpha,\beta,\gamma)$

Table C.1: Some properties of spherical harmonics in Racah normalization $C^l_m(\theta,\phi)$ and Wigner D-matrices $D^{(l)}_{mk}(\alpha,\beta,\gamma)$

$$
\begin{aligned}
&= (-1)^J D^{(J)}_{MK}(\alpha,\beta,0)^* \times \\
&\quad \sum_{m_A,m_B} (-1)^{j_A+j_B+j} \langle j,-K|\, j_A m_A; j_B m_B\rangle C^{j_A}_{m_A}(\theta_A,\phi_A) C^{j_B}_{m_B}(\theta_B,\phi_B) \\
&= (-1)^{j_A+j_B+j+J} D^{(J)}_{MK}(\alpha,\beta,0)^* \times \\
&\quad \sum_{m_A,m_B} \langle j,-K|\, j_A m_A; j_B m_B\rangle C^{j_A}_{m_A}(\theta_A,\phi_A) C^{j_B}_{m_B}(\theta_B,\phi_B) \\
&= (-1)^{j_A+j_B+j+J} |\, j_A, j_B, j, -K; J, M\rangle. \qquad \text{(C.1)}
\end{aligned}
$$

The effect of $\hat{P}$ is given by

$$
\begin{aligned}
&\hat{P}|\, j_A, j_B, j, K; J, M\rangle \\
&= \hat{P}\left[D^{(J)}_{MK}(\alpha,\beta,0)^* \sum_{m_A,m_B} \langle jK|\, j_A m_A; j_B m_B\rangle C^{j_A}_{m_A}(\theta_A,\phi_A) C^{j_B}_{m_B}(\theta_B,\phi_B) \right] \\
&= D^{(J)}_{MK}(\pi+\alpha,\pi-\beta,0)^* \times \\
&\quad \sum_{m_A,m_B} \langle jK|\, j_A m_A; j_B m_B\rangle C^{j_A}_{m_A}(\pi-\theta_B,-\phi_B) C^{j_B}_{m_B}(\pi-\theta_A,-\phi_A) \\
&= e^{iM\pi}(-1)^{J+M} D_{MK}(J)(\alpha,\beta,0)^* \times \\
&\quad \sum_{m_A,m_B} \langle jK|\, j_A m_A; j_B m_B\rangle (-1)^{j_A} C^{j_A}_{-m_A}(\theta_B,\phi_B) (-1)^{j_B} C^{j_B}_{-m_B}(\theta_A,\phi_A) \\
&= (-1)^{j_A+j_B+J} D^{(J)}_{MK}(\alpha,\beta,0)^* \times \\
&\quad \sum_{m_A,m_B} \langle jK|\, j_A, -m_A; j_B, -m_B\rangle C^{j_A}_{m_A}(\theta_B,\phi_B) C^{j_B}_{m_B}(\theta_A,\phi_A) \\
&= (-1)^{j_A+j_B+J} D^{(J)}_{MK}(\alpha,\beta,0)^* \times \\
&\quad \sum_{m_A,m_B} (-1)^{j_A+j_B+j} \langle j,-K|\, j_A m_A; j_B m_B\rangle C^{j_A}_{m_A}(\theta_B,\phi_B) C^{j_B}_{m_B}(\theta_A,\phi_A) \\
&= (-1)^{j+J} D^{(J)}_{MK}(\alpha,\beta,0)^* \times \\
&\quad \sum_{m_A,m_B} (-1)^{j_A+j_B+j} \langle j,-K|\, j_B m_B; j_A m_A\rangle C^{j_A}_{m_A}(\theta_B,\phi_B) C^{j_B}_{m_B}(\theta_A,\phi_A) \\
&= (-1)^{j_A+j_B+J} D^{(J)}_{MK}(\alpha,\beta,0)^* \times \\
&\quad \sum_{m_A,m_B} \langle jK|\, j_B m_B; j_A m_A\rangle C^{j_A}_{m_A}(\theta_B,\phi_B) C^{j_B}_{m_B}(\theta_A,\phi_A) \\
&= (-1)^{j_A+j_B+J} |\, j_B, j_A, j, -K; J, M\rangle. \qquad \text{(C.2)}
\end{aligned}
$$

From Eqs. (C.1) and (C.2) we can easily derive the effect of $\hat{P}^* = \hat{E}^*\hat{P} = \hat{P}\hat{E}^*$ on the angular basis to be

$$
\hat{P}^*|\, j_A, j_B, j, K; J, M\rangle = (-1)^J |\, j_B, j_A, j, K; J, M\rangle. \qquad \text{(C.3)}
$$

The effect of the permutation inversion operators on the monomer vibrational basis functions are given by

$$
\begin{aligned}
\hat{E}^*|\, v_A, v_B\rangle &= |\, v_A, v_B\rangle \qquad \text{(C.4)} \\
\hat{P}|\, v_A, v_B\rangle &= \hat{P}\left[\chi_{v_A}(r_A)\chi_{v_B}(r_B)\right]
\end{aligned}
$$

$$\begin{aligned}
&= \chi_{v_A}(r_B)\chi_{v_B}(r_A) \\
&= |\, v_B, v_A\rangle \qquad \text{(C.5)} \\
\hat{P}^*|\, v_A, v_B\rangle &= \hat{E}^*\hat{P}|\, v_A, v_B\rangle \\
&= |\, v_B, v_A\rangle. \qquad \text{(C.6)}
\end{aligned}$$

Since none of the permutation inversion operators changes R, their effect on the dimer vibrational basis functions is trivial:

$$\hat{E}^*|\, v_{AB}\rangle = \hat{P}|\, v_{AB}\rangle = \hat{P}^*|\, v_{AB}\rangle = |\, v_{AB}\rangle. \qquad \text{(C.7)}$$